The Thesis Committee for Tristan C. Moody
certifies that this is the approved version of the following thesis:

Local Estimation of Modeling Error in Multi-Scale Modeling of Heterogeneous Elastic Solids

Committee:

Albert Romkes, Supervisor

Karan S. Surana

Peter W. TenPas

Local Estimation of Modeling Error in Multi-Scale Modeling of Heterogeneous Elastic Solids

by

Tristan C. Moody, B.S.

Presented to the Faculty of the Graduate School of The University of Kansas
in partial fulfillment of the requirements for the Degree of
MASTER OF SCIENCE

Committee:

Albert Romkes, Supervisor

Karan S. Surana

Peter W. TenPas

THE UNIVERSITY OF KANSAS

Defended February 27, 2008

Acknowledgments

I would like to thank my advisor Dr. Albert Romkes, and the other members of my graduate committee: Dr. Karan Surana and Dr. Peter Ten-Pas for their encouragement and support which made it possible for me to complete this work. Additionally, I would like to express my appreciation to the University of Kansas School of Engineering for financial support through the Zimmerman and Strobel Graduate Fellowships.

Most of all, I would like to express my profound appreciation for my fiancée Krista for her surpassing patience and understanding throughout my graduate studies.

Tristan C. Moody

Lawrence, Kansas.

Local Estimation of Modeling Error in Multi-Scale Modeling of Heterogeneous Elastic Solids

Tristan C. Moody, M.S.
The University of Kansas, 2008

Supervisor: Albert Romkes

This thesis presents the results of an investigation toward the development of a new methodology of local estimation of modeling error in the analysis of linear elastostatic problems of heterogeneous solids. Due to the increase in the use of multiphase composites in structural engineering applications in the past three or four decades, the numerical analysis of their mechanical response has accordingly gained importance. However, it is well known that the microscopic heterogeneity of the material data generally leads to computational problems that are beyond practical means.

Several methods have been developed that essentially seek to replace the complex models with surrogate descriptions of the material behavior that lead to computational feasibility. In this work, a relatively recent approach, called *Goal-Oriented Adaptive Modeling* (GOAM), is considered, which was introduced by Oden, et al. [15, 16, 21, 22]. The distinguishing feature in its concept is that it seeks to construct surrogate, multi-scale material models that are capable of providing accurate predictions of the microscopic features of the material response that are of practical interest to the analyst. To do

so, a homogenized surrogate model is first established, using existing classical homogenization techniques, and its response is obtained. A *goal-oriented* assessment is then made of the quality of the solution from the surrogate model by computing estimates of the modeling error in the fine-scale response features that are of interest to the analyst. Depending on the estimated error, the model is accordingly enhanced in an iterative process by including some fine-scale heterogeneous data in a small portion of the domain near the domain of interest.

A crucial aspect of this process is the *error estimate*. For the method to be of practical use, one must be able to verify the accuracy of the predictions of any of the surrogate descriptions. Only then can one accept or reject any of the surrogate descriptions, with or without some fine scale features. In other words: *the estimates are necessary to validate the models.* Current error estimates rely on the solution of a dual problem, related to the quantity of interest of the response. The dual problem in these approaches is defined *globally*, requiring the heterogeneous material data for the entire domain. Thus, the computation of the dual solution is just as prohibitively expensive as the solution of the exact problem. To overcome this, surrogate models have been proposed to compute the dual problem as well, further introducing an inaccuracy into the error estimate.

In this thesis, these problems are resolved by introducing a new, *local* error estimator that can be computed exactly, therefore eliminating the need for expensive global computations and enhancement iterations in the error estimation process. The estimates are only applicable to quantities of interest

involving stresses and gradients of displacement and quantities that can be expressed as *linear* functionals of the material response. A two-dimensional, heterogeneous, linearly elastic beam under bending and tensile loads is used as a model problem to present numerical studies.

Table of Contents

Acknowledgments **iii**

Abstract **iv**

List of Tables **ix**

List of Figures **xi**

Chapter 1. Introduction **1**

1.1 Micro-Mechanical Behavior of Heterogeneous Elastic Solids – Motivation for Research 1

1.2 Modeling of Heterogeneous Materials – Bibliographical Remarks 6

1.3 Goal of Research 9

Chapter 2. Linear Elastostatics Problems **11**

2.1 Model problem 11

2.2 The Variational Formulation 13

Chapter 3. Goal-Oriented Adaptive Modeling (GOAM) **15**

3.1 Initial Surrogate Descriptions – Classical Homogenization . . . 17

3.2 Quantities of Interest 19

3.3 Model Enhancement 20

3.3.1 Local Enhancement 22

3.3.2 Global Enhancement 24

3.3.3 The Adaptive Process 24

Chapter 4. Modeling Error Estimation **30**

4.1 Residual-Based Error Estimation 30

4.2 Error Estimation based on Local Problem Descriptions 36

Chapter 5. Numerical Verifications **45**

5.1 Verification of Modeling Error Estimates 45

5.2 Initial Extention to Stochastic Problems 76

Chapter 6. Concluding Remarks and Future Work **81**
6.1 Major Accomplishments 81
6.2 Limitations and Future Work 84

Appendix **87**

Appendix 1. Development of Homogenized Material Properties **88**

Bibliography **90**

Vita **95**

List of Tables

5.1 Quantity of interest $\mathbf{Q}^x(\mathbf{u})$ for a deterministic problem, applying three enhancements 63

5.2 Quantity of interest $\mathbf{Q}^y(\mathbf{u})$ for a deterministic problem, applying three enhancements 64

5.3 Quantity of interest $\mathbf{Q}^\gamma(\mathbf{u})$ for a deterministic problem, applying three enhancements 65

5.4 Total and relative errors in quantity of interest $\mathbf{Q}^x(\mathbf{u})$ for homogenized solution 66

5.5 Total and relative errors in quantity of interest $\mathbf{Q}^y(\mathbf{u})$ for homogenized solution 67

5.6 Total and relative errors in quantity of interest $\mathbf{Q}^\gamma(\mathbf{u})$ for homogenized solution 68

5.7 Total and relative errors in quantity of interest $\mathbf{Q}^x(\mathbf{u})$ for three enhancements 69

5.8 Total and relative errors in quantity of interest $\mathbf{Q}^y(\mathbf{u})$ with three enhancements 70

5.9 Total and relative errors in quantity of interest $\mathbf{Q}^\gamma(\mathbf{u})$ with three enhancements 71

5.10 Estimates of enhancement errors in quantity of interest $\mathbf{Q}^x(\mathbf{u})$ based on η_0 using three enhancements with effectivity indices . 72

5.11 Estimates of enhancement errors in quantity of interest $\mathbf{Q}^y(\mathbf{u})$ based on η_0 using three enhancements with effectivity indices . 73

5.12 Estimates of enhancement errors in quantity of interest $\mathbf{Q}^\gamma(\mathbf{u})$ based on η_0 using three enhancements with effectivity indices . 74

5.13 Average estimates of enhancement errors in quantity of interest $\mathbf{Q}^x(\mathbf{u})$ using three enhancements with effectivity indices 75

5.14 Quantity of interest $\mathbf{Q}^x(\mathbf{u})$ values for deterministic problem with three enhancements 79

5.15 Total and relative errors in quantity of interest $\mathbf{Q}^x(\mathbf{u})$ for homogenized solution 79

5.16 Total and relative errors in quantity of interest $\mathbf{Q}^x(\mathbf{u})$ for two enhancements 79

5.17 Estimates of enhancement errors in quantity of interest $\mathbf{Q}^x(\mathbf{u})$ based on η_0 using two enhancements with effectivity indices . 80

5.18 Average estimates of enhancement errors in quantity of interest $\mathbf{Q}^x(\mathbf{u})$ using three enhancements with effectivity indices 80

List of Figures

1.1 Examples of composite failure modes 4

2.1 The model problem 12

3.1 An example exact problem 16
3.2 Homogenization of a heterogeneous solid 18
3.3 Partitioning the homogenized surrogate model 21
3.4 A local enhancement problem 22
3.5 A global enhancement problem 23
3.6 A flowchart of the GOAM algorithm 27
3.7 The adaptive process using *global* enhancement 28
3.8 The adaptive process using *local* enhancement 29

5.1 Test problem: a carbon-epoxy composite beam 46
5.2 Subdomain labels and enhancement regions for the test problem 47
5.3 Full finite element mesh 49
5.4 Contour plots of the exact strain fields 50
5.5 Contour plots of the homogenized strain fields 51
5.6 Contour plots of the strain fields after the first enhancement . 53
5.7 Contour plots of the strain fields after the second enhancement 54
5.8 Contour plots of the strain fields after the third enhancement . 55
5.9 Finite element mesh for the dual problem 56
5.10 Contour plots of dual solution – quantity of interest is local average strain ε_{xx} with an inclusion 57
5.11 Contour plots of dual solution – quantity of interest is local average strain ε_{xx} without an inclusion 57
5.12 Contour plots of dual solution – quantity of interest is local average strain ε_{yy} with an inclusion 58
5.13 Contour plots of dual solution – quantity of interest is local average strain ε_{yy} without an inclusion 58
5.14 Contour plots of dual solution – quantity of interest is local average strain γ_{xy} with an inclusion 59

5.15 Contour plots of dual solution – quantity of interest is local average strain γ_{xy} without an inclusion 59

Chapter 1

Introduction

This document presents the results of a detailed investigation toward a new, local method of estimating modeling error in the multi-scale modeling of heterogeneous elastic solids. In the following, the motivation for the research efforts and a bibliographic background of current approaches and methodologies in this area are given in Sections 1.1 and 1.2, respectively.

1.1 Micro-Mechanical Behavior of Heterogeneous Elastic Solids – Motivation for Research

The use of heterogeneous elastic solids—*i.e.* composites—in engineering is, strictly speaking, hardly a new development. Many historic building materials are considered *fibrous composites*, that is, multiphasic materials consisting of one or more reinforcing *fiber* phases surrounded and supported by a *matrix* phase. Perhaps the most common example of such a composite, and a naturally occuring one, is wood, which consists of cellulose fibers in a lignin matrix. The use of man-made composites dates back to ancient Egypt where the papyrus plant was used to make ropes, sails, baskets, and–most famously–paper, as well as the use of straw-reinforced mud bricks, a precursor to today's reinforced concrete. Beginning in the 1950s, however, the development of advanced fibers such as boron and carbon has led to an explosion in the use of

composites in engineering. Today's advanced composites are much stiffer and stronger for their weight than traditional engineering materials such as steel and aluminum, and with the proper selection and processing of the constituent components, the material properties can be tailored to the needs of specific applications. These advantages, along with the ability to construct complex geometry far more easily than with traditional engineering materials, has encouraged increasingly widespread use of these materials. A particular example is in the aerospace industry, where designs are typically weight-critical, or in athletics and recreation, where the additional strength of these materials allows the creation of lighter, longer-lasting skis, tennis rackets, helmets, and the like.

As the application of these heterogeneous materials has become more common, especially in the use of critical structural components, it becomes necessary to understand the mechanics of these materials. Traditional engineering materials are typically considered to be homogeneous, and stresses and strains are generally smooth over the entire structure, allowing relatively easy predictions of the behavior of these materials. Composite structures, however, are highly heterogeneous, and material properties vary enormously over length scales as small as a few micrometers. This spacial variability creates a corresponding variability in–and local concentration of–stresses and strains when these structures are placed under load. Because the length scale of this variablilty is often several orders of magnitude smaller than that of the structure as a whole, it is often exceedingly difficult, if not impossible, to precisely predict this micro-mechanical behavior for an entire composite structure through computational means.

For traditional, homogeneous engineering materials, critical material properties relating to design are well-known. For example, the point at which a particular aluminum alloy will permanently deform, or the load under which a certain high-carbon steel will fracture, are relatively consistent from sample to sample and across several length scales, due to the homogeneity of these materials. For composite materials, however, the *in situ* loading for a composite structure that will create failure-inducing stresses and strains is dependent on numerous factors, including:

- the volume fractions of the constituents,
- the arrangement of the fibers in the matrix,
- the shape of the fibers,
- residual stresses from the formation of the composite, and
- thermal stresses due to differences in thermal expansion coefficients between the fiber and the matrix.

Likewise, failure modes for traditional materials differ from those for composites. In traditional materials, failure initiates due to microcracks, expanding and joining together in rapid succession to form a fracture. Due to the homogeneity of these materials, the location and nature of these fractures is relatively consistent. In composites, however, failure does not typically occur in a uniform way–in fact, micro-scale failures may occur for a sigficant amount of time and loading before a visible macro-scale failure is evident. These micro-scale failures are consist of some combination of the following failure modes, as described by Herakovich [9] (see Figure 1.1):

Figure 1.1: Examples of composite failure modes

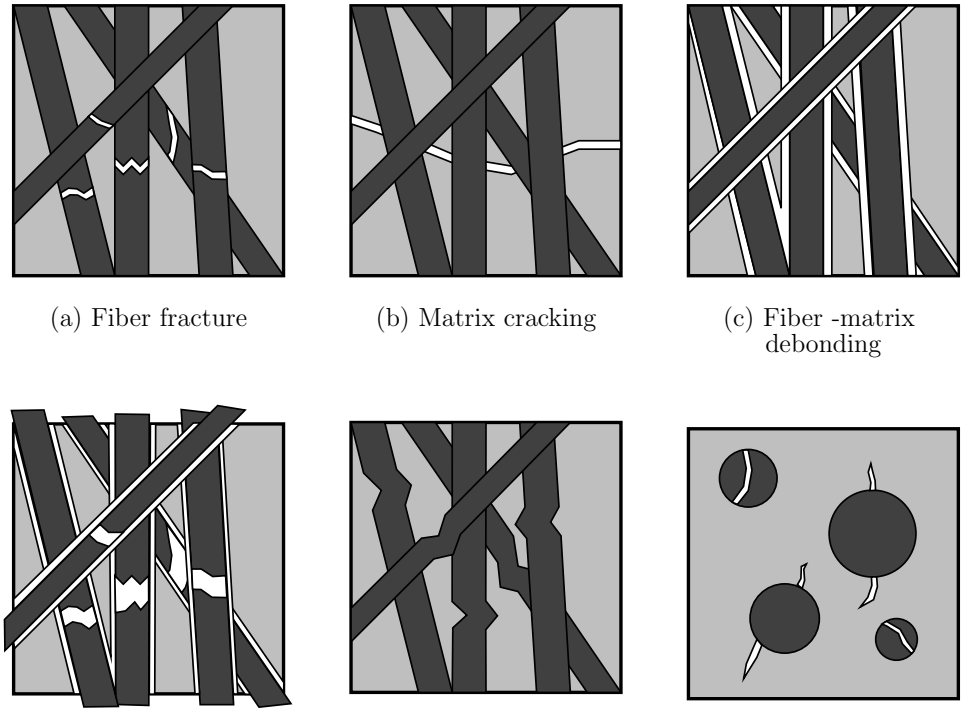

(a) Fiber fracture

(b) Matrix cracking

(c) Fiber -matrix debonding

(d) Fiber pullout

(e) Fiber kinking

(f) Fiber splitting and radial interface cracking

(a) fiber fracture, in which the ultimate tensile strength of individual fibers is exceeded, causing transverse fractures that cleave individual fibers,

(b) matrix cracking, in which the ultimate tensile strength of the matrix material is exceeded at some point,

(c) fiber/matrix debonds, in which the bond connecting the fiber to the matrix is broken,

(d) fiber pullout, a combination of fiber fracture and fiber/matrix debonds,

(e) fiber kinking, caused by compressive stresses that exceed the buckling strength of the fiber, and

(f) radial interface cracking and fiber splitting, when stresses within or surrounding a fiber exceed ultimate values.

Though average properties for composites can be determined that reflect, on some level, the macroscopic properties of the material, such as bulk elasticity and ultimate strength, these properties, lacking information on the heterogeneity of the material, cannot provide information on failure mechanisms for a particular situation, nor do they reflect the progressive change in the macro-scale material behavior caused by micro-scale damage. Indeed, the failure of a handful of individual fibers may not cause catastrophic failure of the material, but without the micro-scale information, neither the occurrence nor the effect of this damage can be predicted.

It is to this end, then that a reliable and computable method of including micro-scale information in the prediction of the response of heterogeneous

elastic solids is necessary.

1.2 Modeling of Heterogeneous Materials – Bibliographical Remarks

The simulation of the elastostatic behavior of heterogeneous materials such as composites has until recently been done predominantly by determining effective properties, *i.e.*, averaged or smoothened bulk properties that are only sensitive to the macro-scale behavior of the reponse of the material to external loads. These properties are traditionally what are determined by standard laboratory tests, such as the tensile, compressive, or torsional loading of rods. A major focus of research has been to establish bounds on these material parameters. Indeed, some of the most highly regarded work in mechanics of materials over the past several decades is devoted to this particular topic. Some particularly well-known examples, the works of Hill [10]; Hashin and Shtrikman [8], Balendran and Nemat-Nasser [1]; and Nemat-Nasser and Hori [11] are noted. These averaging methods inspired new mathematical research into the homogenization of partial differential equations. Of particular interest are the works of Bensoussan *et al.* [2] and Sanchez-Palencia [18], in which asymptotic expansions of the response are used, based on the assumption that the microstructure is periodic. More recently, modern imaging and computational methods have been utilized to determine effective properties of actual specimens, using techniques such as the Voronoi Cell Finite Element Method as in the works of Ghosh *et al* [5, 6]; Boundary Element Method, as used by Fu *et al* [3]; and the adaptation of digital data obtained from Computerized X-Ray Tomography, as done by Terada *et al* [20].

Similarly, a multi-scale approach has been adopted in the works of Guedes and Kikuchi [7] and Terada and Kikuchi [19]. These works use the aforementioned homogenizaton techniques and include asymptotic perturbations to account for micro-mechanical behavior. A similar approach was used by Ghosh, Lee, and Moorthy [4] to study elasto-plastic behavior.

All of the aforementioned approaches are noted by their restriction to materials with periodic microstructures. In the past several years, a new approach has been developed that allows the actual micro-mechanical features of materials to be used to predict the micro-scale behavior. This approach, known as *Hierarchical Modeling*, involves the use of only enough micro-scale information to determine vital features of the macro-scale response to within preset accuracy levels. In this approach, homogenization methods are used, but only as an intermediate step in a broader algorithm. Oden and Zohdi [17] and Zohdi *et al* [23, 24] presented hierarchical adaptive modeling method for elastostatic problems based on bounds of the modeling error in terms of its global quantities, such as the energy, or L^2, norm of the error. The goal of this method is to provide a hierarchy of descriptions of the physical properties that can be used in different subdomains of the material. In this approach, *a posteriori* error estimates of the modeling error are used to determine the level of complexity required for each subdomain.

The original method was known as the *Homogenized Dirichlet Projection Method* and involves two different levels of description: a homogenized, macro-scale description and the exact micro-scale description. The algorithm proceeds thusly: an initial approximation is made using homogenized prop-

erties throughout the entire domain; then, *a posteriori* error estimates of the modeling error are determined and an iterative process is started in which critical regions of the material have the fine-scale problem solved using the homogenized solution as a Dirichlet boundary condition on the boundary of the subdomain. This iterative proces continues by including progressively more critical regions into the micro-scale analysis until the error estimate meets tolerances set by the user.

Where the previous procedure uses *global* error estimates–that is, energy or L^2 norms of the error–Oden and Vemaganti [16, 15, 21, 22] advanced this work by introducing the *Goal-Oriented Adaptive Local Solution Algorithm*, where error estimates in *local* quantities of interest are used. These estimates allow the user to use *goal-oriented* adaptive strategies, in which a model is adapted to yield accurate predictions of user-specified features of the response.

As mentioned previously, these works were created in the context of elastostatic proglems. Recently, an extension of this approach to general goal oriented engineering applications has been proposed by Oden and Prudhomme [12, 13], using a residual-based analysis of the modeling error.

It is crucial to this method, then, to derive some way to estimate the error in these solutions, since the actual modeling error obviously cannot be determined. Most error estimates involve the solution of some dual problem, through which the error in the desired quantity of interest can be extracted from the surrogate solution. These dual problems, however, are typically global in nature, requiring fine-scale information over the entire domain and thus are usually just as difficult to solve as the exact problem. Consequently, the

dual problem must itself be approximated by some surrogate model as well, with progressive enhancements applied much in the same way as in the main problem. Thus, not only must an adaptive modeling algorithm be applied to the exact problem, it must be applied to the dual problem as well, which is global in nature, greatly increasing computational expense and reducing accuracy.

1.3 Goal of Research

The primary goal of this research is the development of an improved methodology for estimation of modeling error for linear elastostatics problems of heterogeneous solid materials, *i.e.* composites. This methodology will be residual-based and will employ *local*, rather than global, integrals, significantly reducing the computational expense of the error estimate. The development of this methodology involves the following objectives:

- The development of a variational, *i.e.* integral statement of a dual problem based on local descriptions
- The consideration of quantities of interest that are linear functionals of the micro-mechanical response, *e.g.,* average tensile strain in a small subdomain.
- The development of a modeling error estimate that only employs **local** mechanical information and dual solutions, hence establishing estimators that are *tractable*.

- Preliminary investigation of methods for local enhancements to the homogenized model.

To present the development of this methodology, this document is organized as follows:

- **Chapter 2** explains the model problem used in this research and describes the formulation used to solve it.
- **Chapter 3** then describes the adaptive algorithm used to develop a computable surrogate problem that provides a desired level of accuracy in terms of a quantity of interest.
- **Chapter 4** presents both the current error estimation methodology in use and the newly developed local error estimate
- **Chapter 5** presents numerical verification results, and
- **Chapter 6** presents conclusions and projected future research topics.

Chapter 2

Linear Elastostatics Problems

In this chapter, the general linear elastostatics problem is presented. The model problem and important notations are introduced in Section 2.1. A variational formulation of this problem, suitable for finite element analysis, is then given in Section 2.2.

2.1 Model problem

An open, bounded domain $\Omega \subset \mathbb{R}^d$, $d = 1, 2, 3$ is considered, as shown in Figure 2.1, containing a linearly elastic solid material. The boundary $\partial\Omega = \overline{\Gamma_t \cup \Gamma_u}$, $\Gamma_t \cap \Gamma_u = \varnothing$, $meas(\Gamma_t) > 0$, $meas(\Gamma_u) > 0$, with Γ_u and Γ_t representing the portions of the boundary $\partial\Omega$ on which displacements and tractions are specified, respectively. This solid body is subjected to traction $\mathbf{t}$ on Γ_t and a distributed volumetric body load $\mathbf{f}$. Additionally, a zero displacement is prescribed on Γ_u.

It is assumed that the body is composed of a multi-phase, composite, linearly elastic material with highly oscillatory material properties, as shown in Figure 2.1. Let $\mathbf{u}$ denote the displacement vector field defined on Ω, $\nabla\mathbf{u}$ be its spatial gradient, $\nabla\cdot\mathbf{x}$ be the divergence of some tensor or vector quantity $\mathbf{x}$, and $\cdot$ denote the inner product. Then, the Cauchy stress tensor σ satisfies the linear constitutive equation $\sigma = \mathbf{E}\varepsilon$, where ε is the strain tensor and $\mathbf{E} = \mathbf{E}(\mathbf{x})$

Figure 2.1: The model problem

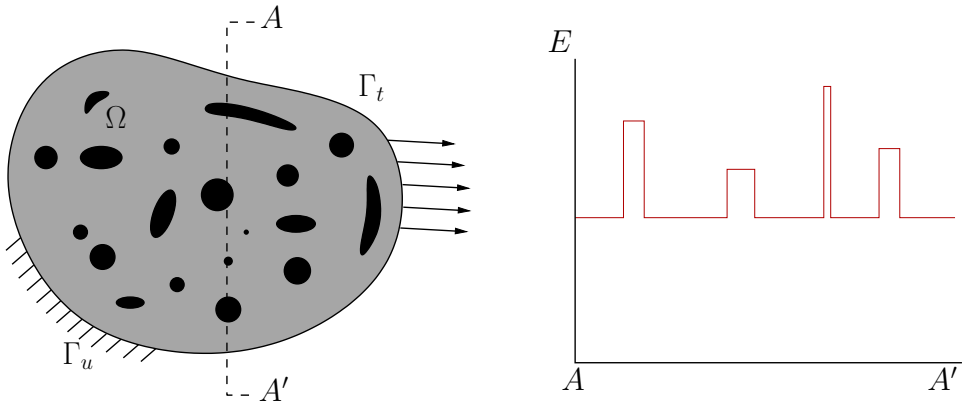

denotes the 4^{th} order elasticity tensor, whose coefficients satisfy the following symmetry and ellipticity conditions:

$$E_{ijkl}(\mathbf{x}) = E_{jikl}(\mathbf{x}) = E_{ijlk}(\mathbf{x}) = E_{klij}(\mathbf{x})$$

$$\alpha_0\, \xi_{ij}\xi_{ij} \leq E_{ijkl}\, \xi_{ij}\xi_{kl} \leq \alpha_1\, \xi_{ij}\xi_{ij},$$

$$\alpha_0,\ \alpha_1 \in \mathbb{R}, \quad \alpha_0 > 0, \quad \alpha_1 > 0$$

The deformations in the material are assumed to be small. Hence the strain-displacement relations are linear:

$$\varepsilon = \frac{1}{2}\left(\nabla \mathbf{u} + (\nabla \mathbf{u})^T\right)$$

Thus, the linear eleastostatics problem can then be formulated in terms of the following classical boundary value problem:

$$\boxed{\begin{array}{c} \text{Find } \mathbf{u} \text{ such that:} \\ -\nabla \cdot (\mathbf{E}\nabla \mathbf{u}) = \mathbf{f} \quad \text{in } \Omega, \\ \mathbf{E}\nabla \mathbf{u} \cdot \mathbf{n} = \mathbf{t} \quad \text{on } \Gamma_t, \\ \mathbf{u} = \mathbf{0} \quad \text{on } \Gamma_u, \end{array}} \tag{2.1}$$

where $\mathbf{n}$ denotes the unit normal to $\partial\Omega$.

2.2 The Variational Formulation

The solution to the problem in (2.1) can rarely—in fact, almost never—be solved analytically. Commonly, it is approximated by computing finite element discretizations of its equivalent formulation. This variational formulation can be obtained in several ways, *e.g.*, using a Least Squares approach or a Galerkin approach. Because the differential operator in (2.1) is self-adjoint, a stable, non-degenerate–or Variationally Consistent–formulation is possible using the Galerkin Method with Weak Form (GMWF). Let the space of test functions be

$$V = \left\{ \mathbf{v} : \int_\Omega \mathbf{E}\nabla\mathbf{v} : \nabla\mathbf{v} \mathrm{d}\mathbf{x} < \infty, \quad \gamma_0(\mathbf{v})_{|\Gamma_u} = 0 \right\}, \tag{2.2}$$

where $\gamma_0 : H^1(\Omega) \to H^{1/2}(\partial\Omega)$ is the zeroth-order trace operator. Then multiplying both sides of the first equation in (2.1) by a test function $\mathbf{v} \in V$ and integrating using Green's identity yields the variational form:

$$\boxed{\begin{array}{c} \text{Find } \mathbf{u} \text{ such that:} \\ B(\mathbf{u}, \mathbf{v}) = F(\mathbf{v}), \quad \forall \mathbf{v} \in V, \end{array}} \tag{2.3}$$

where,

$$\begin{aligned} B(\mathbf{u}, \mathbf{v}) &= \int_\Omega \mathbf{E}\nabla\mathbf{u} : \nabla\mathbf{v} \mathrm{d}\mathbf{x}, \\ F(\mathbf{v}) &= \int_\Omega \mathbf{f} \cdot \mathbf{v} \mathrm{d}\mathbf{x} + \int_{\Gamma_t} \mathbf{t} \cdot \mathbf{v} \mathrm{d}s. \end{aligned} \tag{2.4}$$

Remark 2.2.1. A variational form based on a least-squares formulation is not considered in this thesis but will be pursued in future research efforts (see Section 6.2).

Chapter 3

Goal-Oriented Adaptive Modeling (GOAM)

The accomplishments of this thesis work are essentially a crucial contribution to the GOAM method [15, 16, 21, 22]. This chapter provides a more detailed description of this methodology and elaborates on all of the steps involved. Section 3.1 introduces the homogenized description of the material, which is used as an initial surrogate model in GOAM. The criteria for model adaptation are introduced in Section 3.2. Section 3.3 then concludes with a brief discussion of the successive model enhancements of the homogenized description.

To illustrate the approach and steps of the GOAM method, a model problem is considered as depicted in Figure 3.1. The problem concerns the elasto-static response of a U-shaped heterogeneous elastic solid. The structure is subject to applied uniform tractions $\mathbf{t}$ at the top edge and is fixed at the bottom edge.

3.1 Initial Surrogate Descriptions – Classical Homogenization

Following classical approaches, the GOAM method, as proposed by Oden *et al* [15, 16, 21, 22], acknowledges that the full micromechanical response of heterogeneous solids such as engineering composites cannot be re-

Figure 3.1: An example exact problem

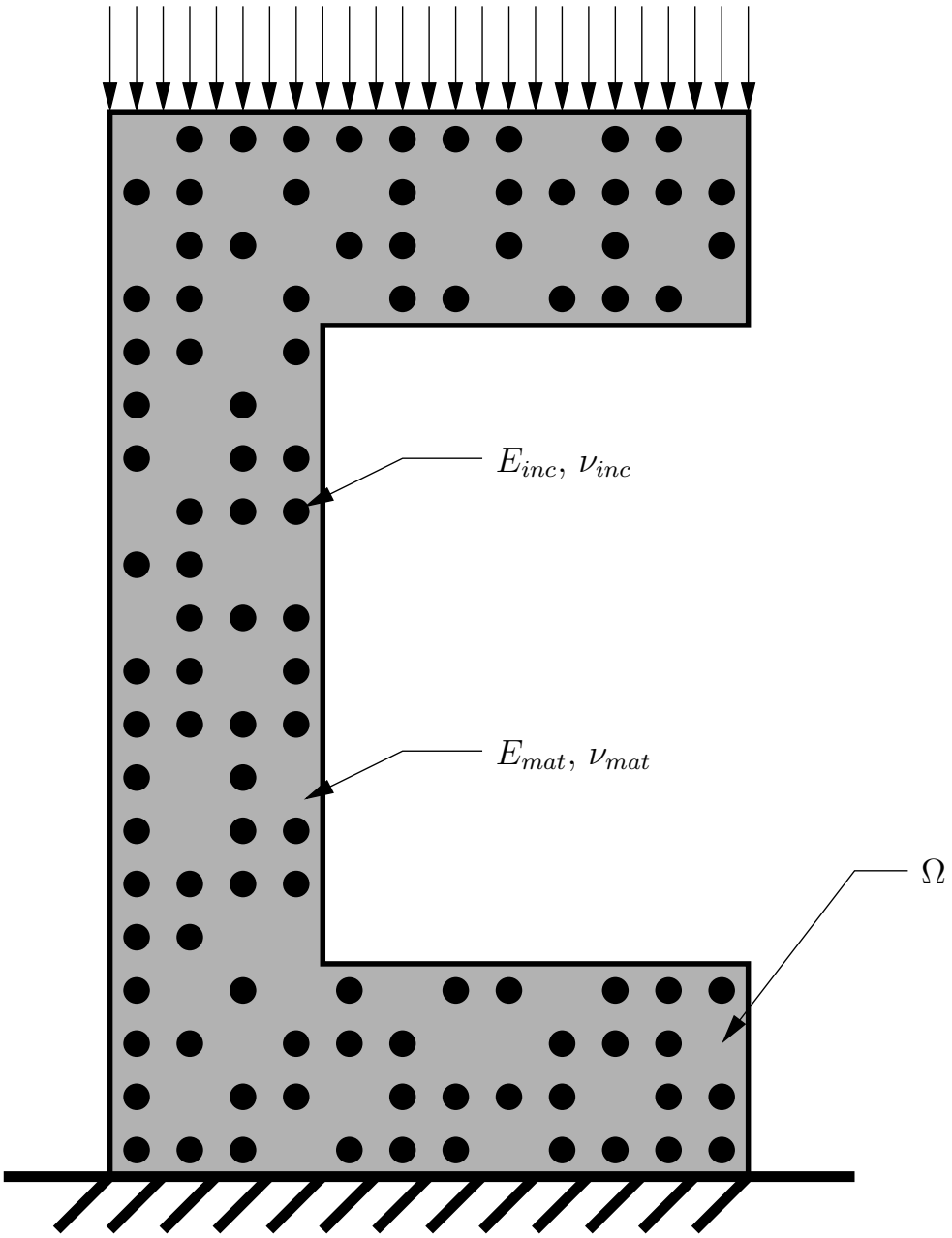

Figure 3.2: Homogenization of a heterogeneous solid

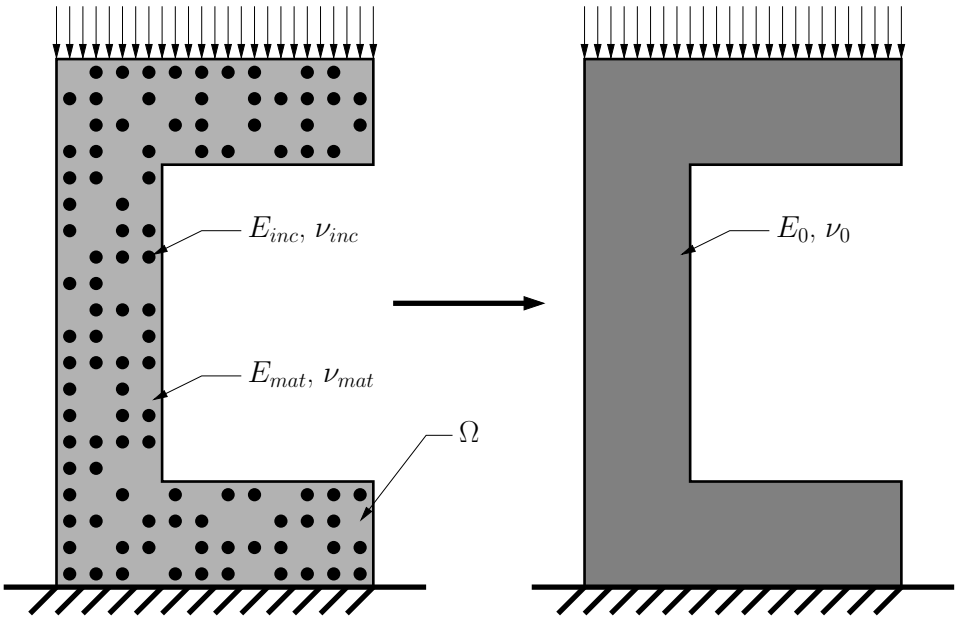

solved completely. The complexity of the microstructure would require numerical discretizations, *e.g.* Finite Element approximations, involving numbers of degrees of freedom that easily exceed available computational resources. Hence, the GOAM method employs classical homogenization techniques to establish an initial surrogate mathematical model (see Figure 3.2). As mentioned in Chapter 1, there are several approaches for achieving averaged or effective material properties.

In this work, average values of the Hashin-Shtrikman [8] upper and lower bounds (see Appendix 1 for a discussion on how these values are obtained) are used to establish averaged, effective material coefficients $E_{0,ijkl}$, yielding a homogenized elasticity tensor $\mathbf{E}_0$. Based on the homogenized material description $\mathbf{E}_0$, one can then seek the corresponding homogenized material

response $\mathbf{u}_0$, which is a solution to the following homogenized version of (2.1):

$$\boxed{\begin{array}{l}\text{Find } \mathbf{u}_0 \text{ such that:} \\ \qquad\qquad -\nabla\cdot(\mathbf{E}_0\nabla\mathbf{u}_0) = \mathbf{f} \quad \text{in } \Omega, \\ \qquad\qquad \mathbf{E}_0\nabla\mathbf{u}_0\cdot\mathbf{n} = \mathbf{t} \quad \text{on } \Gamma_t, \\ \qquad\qquad \mathbf{u}_0 = \mathbf{0} \quad \text{on } \Gamma_u,\end{array}} \tag{3.1}$$

By applying a Galerkin with Weak Form approach, its equivalent variational formulation is governed by:

$$\boxed{\begin{array}{l}\text{Find } \mathbf{u}_0 \text{ such that:} \\ \qquad\qquad B_0(\mathbf{u}_0,\mathbf{v}) = F(\mathbf{v}), \quad \forall\mathbf{v}\in V,\end{array}} \tag{3.2}$$

where,

$$\begin{aligned} B_0(\mathbf{u}_0,\mathbf{v}) &= \int_\Omega \mathbf{E}_0\nabla\mathbf{u}_0 : \nabla\mathbf{v}\mathrm{d}\mathbf{x}, \\ F(\mathbf{v}) &= \int_\Omega \mathbf{f}\cdot\mathbf{v}\mathrm{d}\mathbf{x} + \int_{\Gamma_t}\mathbf{t}\cdot\mathbf{v}\mathrm{d}s. \end{aligned} \tag{3.3}$$

3.2 Quantities of Interest

The homogenized models, although generally computable, yield reasonably accurate predictions of macroscopic features of the material response. As discussed in Section 1.2, they do not provide reliable information on local, micromechanical response features that are crucial in micromechanical failure mechanisms. Thus, depending on the interest and motivation of the analyst, the homogenized predictions are not necessarily satisfactory.

To provide a rigorous means to accept or reject the surrogate solution, that is, to *validate* the model, the GOAM method introduces the notion of the quantities of interest, in an effort to include critical microscopic features of the response into the analysis and implement them as goals of the adapive modeling process. Mathematically, this is extablished by expressing these quantities in terms of functionals $\mathbf{Q} : V \to \mathbb{R}$ of the material response $\mathbf{u}$. Of particular interest in this thesis work are *micro*mechanical features such as:

- The average axial strain in a small subdomain $\omega \in \Omega$:

$$\mathbf{Q}(\mathbf{u}) = \frac{1}{|\omega|}\int_{\omega} \varepsilon_{xx}(\mathbf{u})\mathrm{d}\mathbf{x} = \frac{1}{|\omega|}\int_{\omega} (\nabla \mathbf{u}\mathbf{e}_x \cdot \mathbf{e}_x)\mathrm{d}\mathbf{x} = \frac{1}{|\omega|}\int_{\omega} \frac{\partial u_x}{\partial x}\mathrm{d}\mathbf{x} \quad (3.4)$$

  where $|\omega|$ represents the area of ω.

- The average shear stress in a small subdomain $\omega \in \Omega$:

$$\mathbf{Q}(\mathbf{u}) = \frac{1}{|\omega|}\int_{\omega} \tau_{xy}(\mathbf{u})\mathrm{d}\mathbf{x} = \frac{1}{|\omega|}\int_{\omega} \left(\mathbf{E}\nabla \mathbf{u}(\mathbf{e}_x) \cdot (\mathbf{e}_y)\right)\mathrm{d}\mathbf{x} \quad (3.5)$$

- The total reaction force in the y-direction on a Dirichlet portion of the boundary $\Gamma_u \in \partial\Omega$:

$$\mathbf{Q}(\mathbf{u}) = \int_{\Gamma_u} \mathbf{t}(\mathbf{u}) \cdot \mathbf{e}_y \mathrm{d}\mathbf{s} = \int_{\Gamma_u} (\mathbf{E}\nabla \mathbf{u} \cdot \mathbf{n}) \cdot \mathbf{e}_y \mathrm{d}\mathbf{s} \quad (3.6)$$

The quantity of interest can be a nonlinear functional on V to be suitable for this method, but for the scope of this research, only linear quantities of interest are addressed.

3.3 Model Enhancement

Upon establishing the homogenized solution $\mathbf{u}_0$, the GOAM method validates the homogenized model by computing estimates of the modeling error in terms of the quantities of interest, *i.e.* $\mathbf{Q}(\mathbf{u}) - \mathbf{Q}(\mathbf{u}_0)$. Details on the error estimation process are provided in Chapter 4.

In case the estimates exceed a user-set error tolerance, α_{tol}, the surrogate model is rejected and an iterative process of enhancements of the homogenized model is started. The enhancement is commonly implemented by including part of the *exact* micromechanical features of the material. There is no unique way to this, and to date, this remains an open issue. (See also the comments in Chapter 6 on future work). Oden *et al* [14] provide two alternatives: local and global enhancement. In both approaches, the domain Ω is partitioned into subdomains ω_k, as demonstrated in Figure 3.3. For each subdomain, indicators of its contribution to the modeling error are computed. Those regions with the highest contribution, ω_{crit}, are subsequently considered for model enhancement.

3.3.1 Local Enhancement

In local enhancement, as illustrated in Figure 3.4, a local problem is defined in the critical region ω_{crit} by solving the exact elastostatic PDE in ω_{crit} and applying the homogenized solution $\mathbf{u}_0$ as a prescribed Dirichlet condition on the boundary $\partial\omega_{crit}$, *i.e.*:

Figure 3.3: Partitioning the homogenized surrogate model

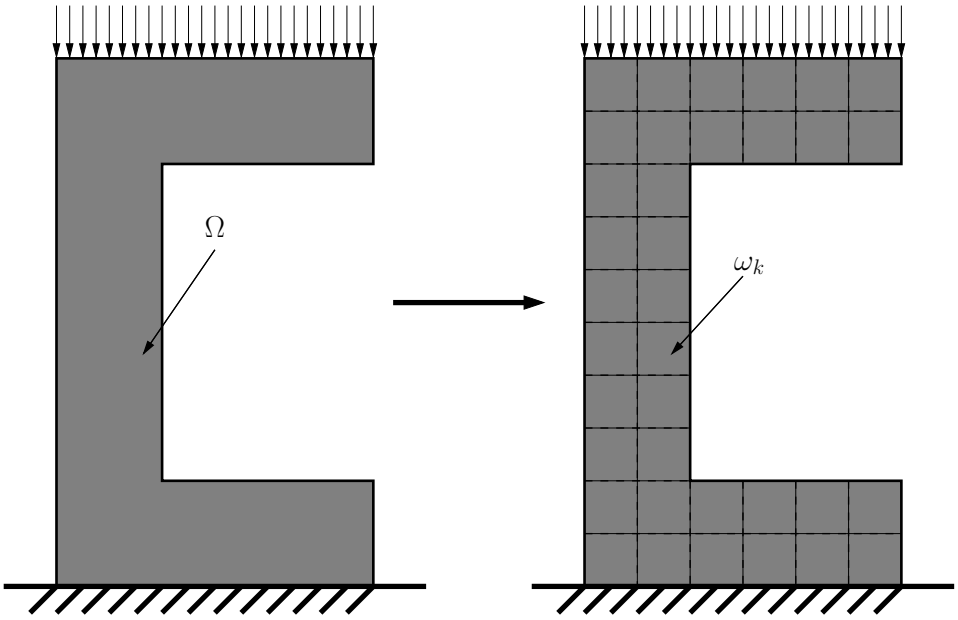

Figure 3.4: A local enhancement problem

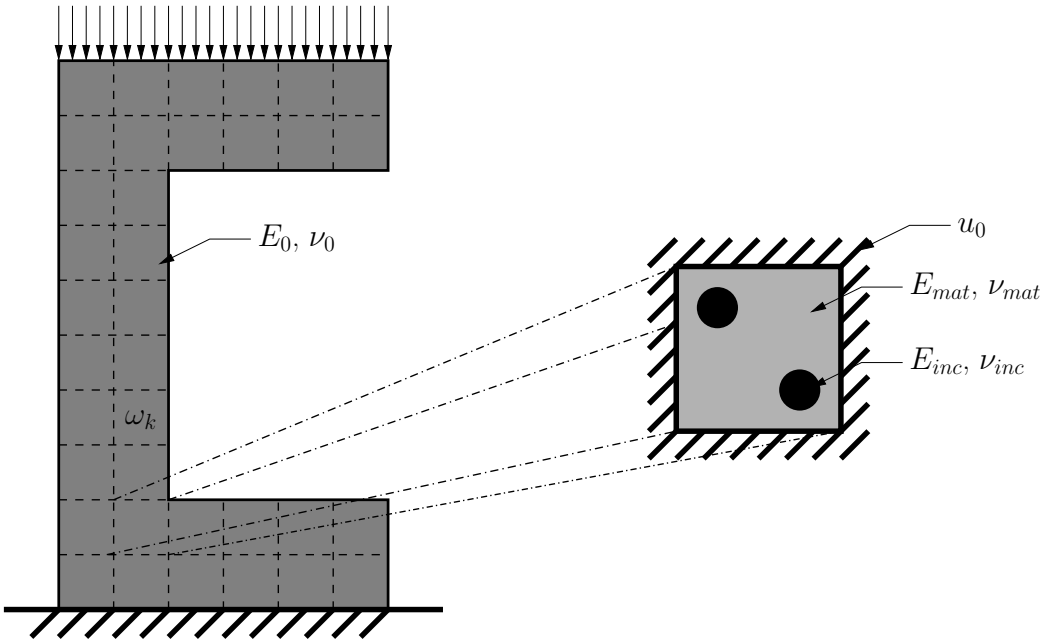

Find $\tilde{\mathbf{u}}$ such that:

$$\begin{aligned} -\nabla \cdot (\mathbf{E}\nabla\tilde{\mathbf{u}}) &= \mathbf{f} \quad \text{in } \omega_{crit}, \\ \tilde{\mathbf{u}} &= \mathbf{u}_0 \quad \text{on } \partial\omega_{crit} \end{aligned} \tag{3.7}$$

The local enhancement technique benefits from greatly reduced computational expense, as the domain of computation is much smaller than the global problem. However, this is not without its drawbacks, as this method effectively decouples the problem from the global domain, preventing the local response from affecting the solution field in the neighboring subdomains, creating accuracy issues and affecting the choice of subdomains to add to the enhancement. In addition, since $\mathbf{u}_0 \neq \mathbf{u}$ on $\partial\omega_{crit}$, the Dirichlet condition in itself has error that pollutes the local problem. In practical application, ω_{crit} must be substantially large for this error to diffuse and not corrupt predictions in ω, resulting in an increase in computational expense

3.3.2 Global Enhancement

In global enhancement, an enhanced problem is defined that considers the entire domain Ω, but in which the exact material properties are applied in the critical domain ω_{crit} and the homogenized properties are applied outside (see Figure 3.5). This leads to an enhanced surrogate description of the material properties:

$$\tilde{\mathbf{E}}(\mathbf{x}) = \begin{cases} \mathbf{E}_0 & \text{for } \mathbf{x} \in \Omega \backslash \omega_{crit} \\ \mathbf{E} & \text{for } \mathbf{x} \in \omega_{crit} \end{cases} \tag{3.8}$$

. The problem is then solved in Ω with the same loading criteria as the homogenized problem:

Figure 3.5: A global enhancement problem

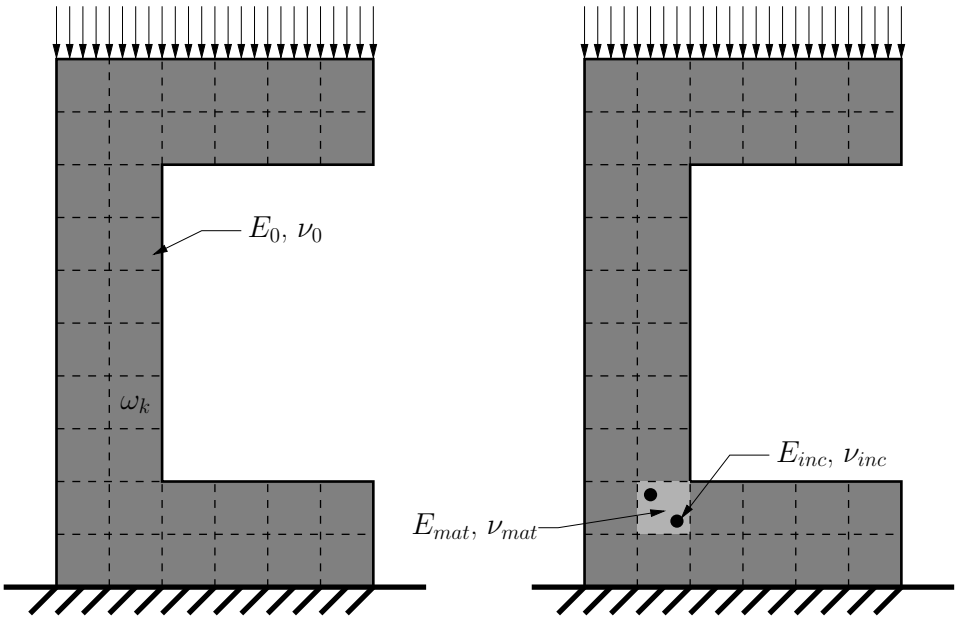

Find $\tilde{\mathbf{u}}$ such that:

$$\begin{aligned} -\nabla \cdot (\tilde{\mathbf{E}} \nabla \tilde{\mathbf{u}}) &= \mathbf{f} \quad \text{in } \Omega, \\ \tilde{\mathbf{E}} \nabla \tilde{\mathbf{u}} \cdot \mathbf{n} &= \mathbf{t} \quad \text{on } \Gamma_t, \\ \tilde{\mathbf{u}} &= \mathbf{0} \quad \text{on } \Gamma_u, \end{aligned} \tag{3.9}$$

Hence, this technique establishes a coupled problem, which improves accuracy but increases computational expense (as the problem is solved globally).

3.3.3 The Adaptive Process

Whether local or global enhancements are employed, the Goal-Oriented Adaptive Modeling method is an iterative process that seeks to establish a surrogate model that can give a reasonably accurate approximation of a pre-

defined goal, or quantity of interest, $\mathbf{Q}(\mathbf{u})$. This adaptive process, illustrated in the flowchart in Figure 3.6 can be summarized in terms of the following steps:

Step 1: The body Ω is partitioned into non-overlapping subdomains ω_k, and the quantity of interest $\mathbf{Q}(\mathbf{u})$ and its associated error tolerance α_{TOL} is assigned.

Step 2: Homogenized material properties are computed (see Appendix 1) and collected into a surrogate elasticity tensor $\mathbf{E}_0$ as described in Section 3.1.

Step 3: The corresponding displacement field $\mathbf{u}_0(\mathbf{x})$ is computed by solving the surrogate problem described in (3.1) (generally by applying a finite element discretization of (3.2)).

Step 4: The modeling error in the quantity of interest, $\mathbf{Q}(\mathbf{u}) - \mathbf{Q}(\mathbf{u}_0)$, is estimated.

Step 5: If the error estimate is less than α_{TOL}, then the analysis **STOPS** and provides the analyst with $\mathbf{Q}(\mathbf{u}_0)$ as the prediction of the response in the quantity of interest.

Step 6: The initial guess of a domain of influence ω_{crit} is determined by taking the union of all subdomains that intersect with the domain upon which the quantity of interest is defined.

Step 7: A new, enhanced problem is constructed by including the exact material properties $\mathbf{E}$ in the domain of influence ω_{crit} according to one of the two enhancement methods described in Subsections 3.3.1 and 3.3.2.

Step 8: The enhanced displacement field $\tilde{\mathbf{u}}_i(\mathbf{x})$, i being the current enhancement number, is solved, according to the enhancement technique chosen (*i.e.* local or global, see Sections 3.3.1 and 3.3.2).

Step 9: The modeling error in the quantity of interest, $\mathbf{Q}(\mathbf{u}) - \mathbf{Q}(\mathbf{u}_i)$, is againestimated.

Step 10: If the error estimate is less than α_{TOL}, then the analysis **STOPS** and provides the analyst with $\mathbf{Q}(\tilde{\mathbf{u}}_i)$ as the prediction of the response in the quantity of interest.

Step 11: If the error estimate exceed the tolerance level, then ω_{crit} is updated by including neighbors of ω_{crit} that have high contribution to the error in terms of computable indicators.

Step 12: The process repeats back to **Step 7**.

A visual illustration of the progression of this adaptive process is shown for global enhancement in Figure 3.7 and for local enhancement in Figure 3.8.

Figure 3.6: A flowchart of the GOAM algorithm

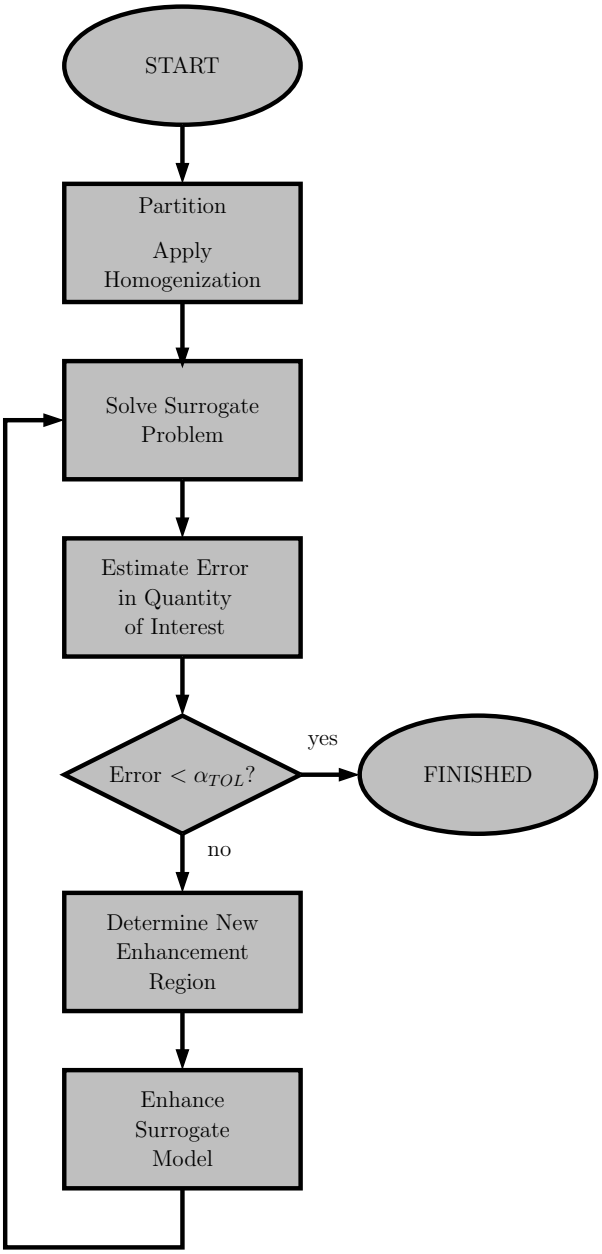

Figure 3.7: The adaptive process using *global* enhancement

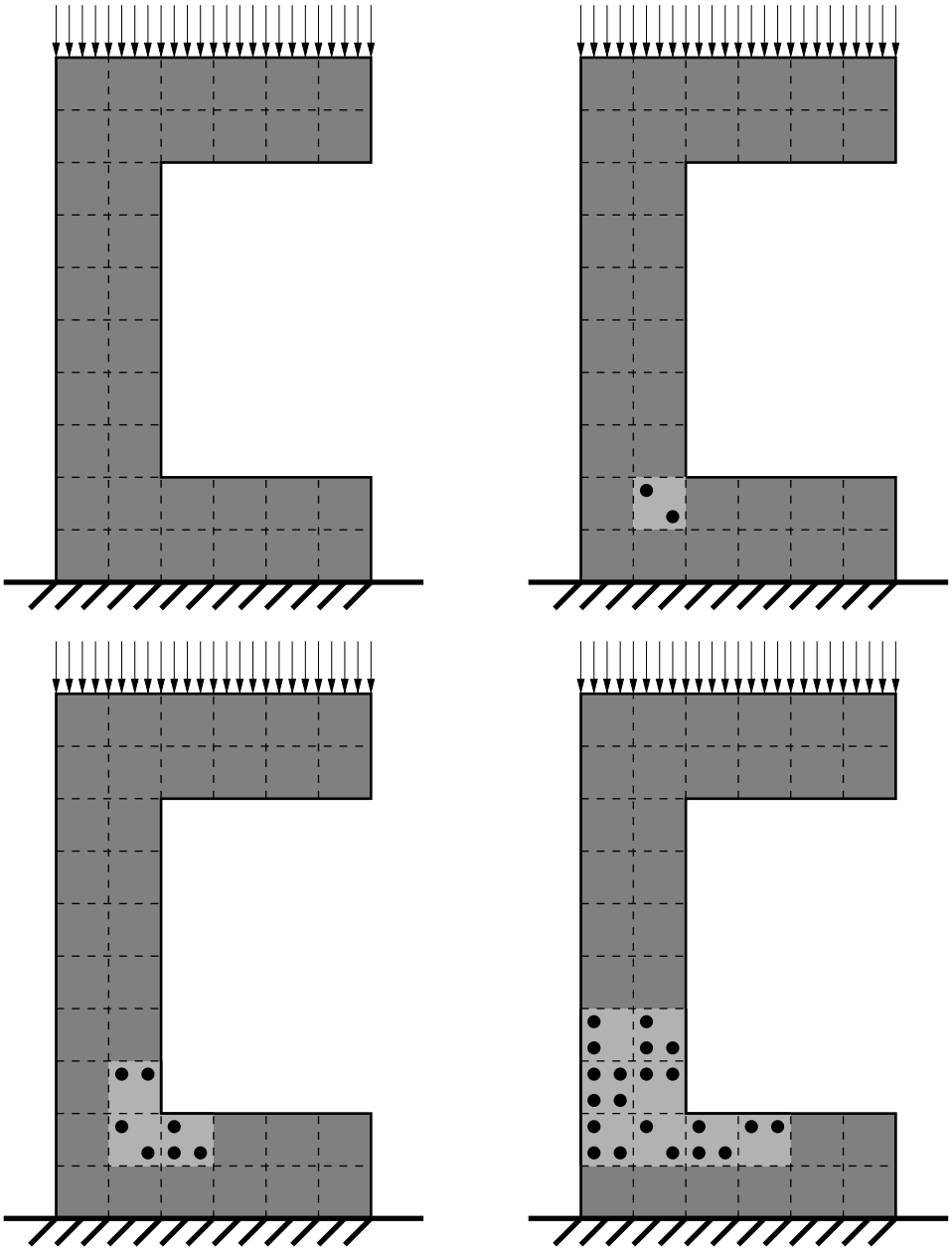

Figure 3.8: The adaptive process using *local* enhancement

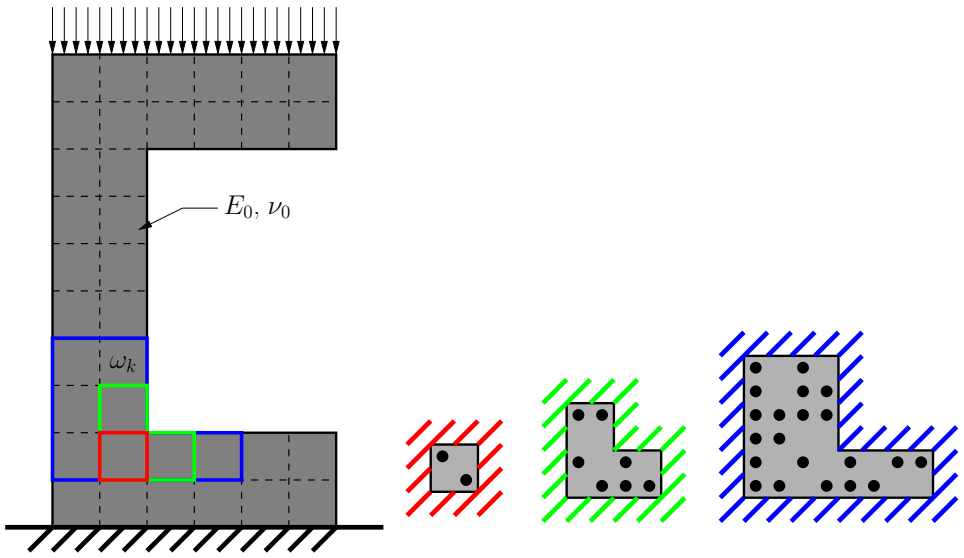

Chapter 4

Modeling Error Estimation

One of the most important elements in the GOAM algorithm is the error estimate, which enables the validation of surrogate models and drives the level to which the model is enhanced. For this algorithm to be practical, an accurate and *computable* error estimate must be derived which will predict the error in the quantity of interest due to differences between the exact and the surrogate models. For the purposes of this research, only quantities of interest are considered that are expressed as **linear** functionals of the response $\mathbf{u}$. To derive error estimates, a residual-based approach is used that was first introduced by Oden and Prudhomme [12]. It was developed to enable estimation of errors by using global descriptions (*i.e.* throughout the entire domain Ω). Details on this approach are given in Section 4.1. The major contribution of this thesis work, a new error estimator that is entirely based on *local* descriptions, is presented in Section 4.2.

4.1 Residual-Based Error Estimation

Given the quantity of interest $\mathbf{Q}(\mathbf{u})$, and noting that $\mathbf{u}$ is the *unique* solution to the boundary value problem (2.3), it is possible to interpret the solution of the boundary value problem in terms of the quantity of interest

equivalently as a constraint minimization problem [12]:

$$\mathbf{Q}(\mathbf{u}) = \inf_{\mathbf{v}\in\mathcal{M}} \mathbf{Q}(\mathbf{v}), \quad \mathcal{M} = \{\mathbf{v} \in V : \ \mathbf{F}(\mathbf{q}) - \mathbf{B}(\mathbf{v}, \mathbf{q}) = 0, \ \forall \mathbf{q} \in V\} \tag{4.1}$$

The solution of this constraint minimization problem is then governed by the minimizer/saddle point $(\mathbf{u}, \mathbf{p})$ of the following Lagrangian

$$\mathbf{L}(\mathbf{v}, \mathbf{q}) = \mathbf{Q}(\mathbf{v}) + \mathbf{F}(\mathbf{q}) - \mathbf{B}(\mathbf{v}, \mathbf{q}) \tag{4.2}$$

(A Lagrange multiplier which addresses the difference in dimension between $\mathbf{Q}(\cdot)$ and the other terms is assumed to be folded into $\mathbf{Q}(\cdot)$ itself)

Thus, it is necessary to find the roots of the Gateaux derivative of the Lagrangian, that is, where:

$$\begin{gathered}\delta\mathbf{L}\big((\mathbf{w}, \mathbf{p}), (\mathbf{v}, \mathbf{q})\big) = \lim_{\theta\to 0} \frac{1}{\theta}\Big[\mathbf{L}\big((\mathbf{w}, \mathbf{p}) + \theta(\mathbf{v}, \mathbf{q})\big) - \mathbf{L}(\mathbf{w}, \mathbf{p})\Big] = 0 \\ \forall (\mathbf{v}, \mathbf{q}) \in V \times V\end{gathered} \tag{4.3}$$

Assuming that $\mathbf{F}(\cdot)$, $\mathbf{B}(\cdot, \cdot)$, $\mathbf{Q}(\cdot)$ are linear functionals simplifies (4.3) to:

$$[\mathbf{Q}(\mathbf{v}) - \mathbf{B}(\mathbf{v}, \mathbf{p})] + [\mathbf{F}(\mathbf{q}) - \mathbf{B}(\mathbf{w}, \mathbf{q})] = 0 \quad \forall (\mathbf{v}, \mathbf{q}) \in V \times V \tag{4.4}$$

where $(\mathbf{v}, \mathbf{q})$ denotes the pair of test functions.

It is important to note that (4.4) can only be satisfied if

$$\boxed{\begin{aligned} \mathbf{B}(\mathbf{w}, \mathbf{q}) &= \mathbf{F}(\mathbf{q}) \quad \forall \mathbf{q} \in V \\ \mathbf{B}(\mathbf{v}, \mathbf{p}) &= \mathbf{Q}(\mathbf{v}) \quad \forall \mathbf{v} \in V \end{aligned}} \tag{4.5}$$

It should be clear that $(4.5)^1$, called the primal problem, is in fact identical to the variational boundary value problem (2.3) and thus has the unique

solution $\mathbf{w} = \mathbf{u}$. Problem $(4.5)^2$ is commonly referred to as the *dual problem* and its solution $\mathbf{p}$ the *dual solution*. The dual solution can be understood as a function indicating the distribution of the sensitivity of the quantity of interest $\mathbf{Q}(\mathbf{u})$ to features of the material model of Ω (*i.e.* high values of $\mathbf{p}$ and/or its derivatives at $\mathbf{x}$ implies high sensitivity). Although generally rarely employed in engineering analysis, one commonly known example of a dual solution is the *Green's function*. The Green's function is in fact the dual solution $\mathbf{p}$ when $\mathbf{Q}(\mathbf{u})$ corresponds to the value of $\mathbf{u}$ at a point $\mathbf{x}_0$, *i.e.*:

$$\mathbf{Q}(\mathbf{u}) = \mathbf{u}(\mathbf{x}_0) = \delta_{\mathbf{x}_0}(\mathbf{u})$$

where $\delta_{\mathbf{x}_0}(\cdot)$ denotes the (irregular) Dirac distribution.

In this thesis work, the situation is considered in which the solution $\mathbf{u}$ is unattainable due to the complexity of the exact problem. Instead, an approximation $\mathbf{z}$ of $\mathbf{u}$ is considered. To quantify its inaccuracy, a primal residual functional $\mathbf{R} : V \times V \to \mathbb{R}$ is introduced as follows:

$$\mathbf{R}(\mathbf{z}, \mathbf{v}) = \mathbf{F}(\mathbf{v}) - \mathbf{B}(\mathbf{z}, \mathbf{v}) \quad \forall \mathbf{v} \in V \tag{4.6}$$

Note that when $\mathbf{z}$ is identical to the exact solution $\mathbf{u}$, the residual functional is then zero.

A dual residual functional $\overline{\mathbf{R}} : V \times V \to \mathbb{R}$ is therefore introduced for any approximation $\mathbf{r}$ of the dual solution $\mathbf{p}$:

$$\overline{\mathbf{R}}(\mathbf{r}, \mathbf{w}) = \mathbf{Q}(\mathbf{w}) - \mathbf{B}(\mathbf{r}, \mathbf{w}) \quad \forall \mathbf{w} \in V \tag{4.7}$$

With the definitions of these functionals in place, the following theorem can be stated:

Theorem 4.1.1. *Let* $\mathbf{z} \in V$ *be any kinematically admissible approximation of* $\mathbf{u}$*, where* $(\mathbf{u}, \mathbf{p})$ *is the solution to* (4.5)*. Then the following equality holds:*

$$\boxed{\mathbf{Q}(\mathbf{u}) - \mathbf{Q}(\mathbf{z}) = \mathbf{R}(\mathbf{z}, \mathbf{p})} \tag{4.8}$$

Proof. Setting $\mathbf{v}$ in $(4.5)^2$ equal to $\mathbf{u}$ and $\mathbf{z}$ respectively yields:

$$\mathbf{Q}(\mathbf{u}) = \mathbf{B}(\mathbf{u}, \mathbf{p})$$

$$\mathbf{Q}(\mathbf{z}) = \mathbf{B}(\mathbf{z}, \mathbf{p})$$

Thus,

$$\mathbf{Q}(\mathbf{u}) - \mathbf{Q}(\mathbf{z}) = \mathbf{B}(\mathbf{u}, \mathbf{p}) - \mathbf{B}(\mathbf{z}, \mathbf{p})$$

Finally, applying the primal problem $(4.5)^1$ gives

$$\mathbf{Q}(\mathbf{u}) - \mathbf{Q}(\mathbf{z}) = \mathbf{F}(\mathbf{p}) - \mathbf{B}(\mathbf{z}, \mathbf{p}) = \mathbf{R}(\mathbf{z}, \mathbf{p})$$

□

In principle, Theorem 4.1.1 and (4.8) enable the quantification of the error $\mathbf{Q}(\mathbf{u}) - \mathbf{Q}(\mathbf{z})$ if the dual solution is known.

Equation (4.8) clearly demonstrates the purpose of the dual solution $\mathbf{p}$. The residual functional $\mathbf{R}(\mathbf{z}, \mathbf{v})$ encompasses and captures the inaccuracy in terms of a global measure (*i.e.* in terms of integrals on Ω). The dual function $\mathbf{p}$, in turn, serves as a *filter* and extracts that part of this global measure that contributes to the error in $\mathbf{Q}(\mathbf{u})$.

But, as said previously, $\mathbf{p}$ is typically impossible to obtain, so if one uses an approximation $\mathbf{r}$ of $\mathbf{p}$, then (4.8) can be rewritten as:

$$\begin{aligned} \mathbf{Q}(\mathbf{u}) - \mathbf{Q}(\mathbf{z}) &= \mathbf{R}(\mathbf{z}, \mathbf{p} - \mathbf{r} + \mathbf{r}) \\ &= \mathbf{R}(\mathbf{z}, \mathbf{r}) + \mathbf{R}(\mathbf{z}, \varepsilon) \end{aligned} \tag{4.9}$$

where $\varepsilon = \mathbf{p} - \mathbf{r}$.

The residual component $\mathbf{R}(\mathbf{z}, \mathbf{r})$ is computable, but the remainder, $\mathbf{R}(\mathbf{z}, \varepsilon)$, since it depends on the unknown $\mathbf{p}$, is not. In most cases, this remainder is of the same order as the computable component and therefore needs to be estimated.

To emphasize and highlight the challenges that lie in estimating the remainder term, consider the case in which the approximation $\mathbf{z}$ is the solution $\mathbf{u}_0$ of the homogenized problem, *i.e.*:

$$\mathbf{B}_0(\mathbf{u}_0, \mathbf{v}) = \mathbf{F}(\mathbf{v}) \tag{4.10}$$

where $\mathbf{B}_0(\cdot, \cdot)$ is as given in (3.3).

The GOAM method generally uses the same surrogate material description to compute an approximation of the dual solution, *i.e.*, consider $\mathbf{r} = \mathbf{p}_0$, where $\mathbf{p}_0$ is the solution of the homogenized problem

$$\mathbf{B}_0(\mathbf{w}, \mathbf{p}_0) = \mathbf{Q}(\mathbf{w})$$

Hence in this case,

$$\mathbf{R}(\mathbf{z}, \varepsilon) = \mathbf{R}(\mathbf{u}_0, \mathbf{p} - \mathbf{p}_0)$$

Applying the definition of the residual (4.6) yields:

$$\mathbf{R}(\mathbf{u}_0, \mathbf{p} - \mathbf{p}_0) = \mathbf{F}(\mathbf{p} - \mathbf{p}_0) - \mathbf{B}(\mathbf{u}_0, \mathbf{p} - \mathbf{p}_0)$$

Subsequently, the solution of the homogenized problem (4.10) changes this into:

$$\mathbf{R}(\mathbf{u}_0, \mathbf{p} - \mathbf{p}_0) = \mathbf{B}_0(\mathbf{u}_0, \mathbf{p} - \mathbf{p}_0) - \mathbf{B}(\mathbf{u}_0, \mathbf{p} - \mathbf{p}_0)$$

Recalling the definitions of $\mathbf{B}(\cdot,\cdot)$ and $\mathbf{B}_0(\cdot,\cdot)$ in (2.4) and (3.3), respectively, allows this expression to be rewritten as:

$$\mathbf{R}(\mathbf{u}_0, \mathbf{p} - \mathbf{p}_0) = \int_{\Omega} \mathbf{E}_0 \nabla \mathbf{u}_0 \cdot \nabla(\mathbf{p} - \mathbf{p}_0) \mathrm{d}\mathbf{x} - \int_{\Omega} \mathbf{E} \nabla \mathbf{u} \cdot \nabla(\mathbf{p} - \mathbf{p}_0) \mathrm{d}\mathbf{x}$$

This residual expression presents two major challenges in its calculation:

- The integrals in this expression are of a global nature, that is, over the entirety of the global domain Ω, at considerable computational expense.
- The dual solution $\mathbf{p}$ cannot be computed exactly, and so surrogate models for the dual problem must be developed, yielding only an approximation, at the expense of a second concurrently-performed model refinement process.

4.2 Error Estimation based on Local Problem Descriptions

This section introduces the derivation of a new error estimate that also enjoys a residual-based approach but is solely based on local descriptions and therefore only requires the solution of (tractable) local dual problems and computation of local integrals. The need to employ surrogate models for the dual problem is eliminated. In many cases, only a single dual problem needs to be solved to estimate modeling errors in many different regions.

In accordance with the philosophy behind the GOAM method (see Chapter 3), the estimation of modeling errors is sought in terms of quantities of interest $\mathbf{Q}(\cdot)$ of the material response. Thus, let $\mathbf{u}(\mathbf{x})$ be the (unknown)

exact fine-scale response of the material and $\tilde{\mathbf{u}}_i$ be any of the (multi-scale) solutions obtained by using the GOAM method. Then the error $\mathbf{Q}(\mathbf{u}) - \mathbf{Q}(\tilde{\mathbf{u}}_i)$ is sought.

First, it is important to note that if $\mathbf{u}_0$ is the (initial) homogenized solution (see Section 3.1), then the error can be decomposed as follows:

$$\mathbf{Q}(\mathbf{u}) - \mathbf{Q}(\mathbf{u}_i) = \underbrace{\mathbf{Q}(\mathbf{u}) - \mathbf{Q}(\mathbf{u}_0)}_{\text{to be estimated}} + \underbrace{\mathbf{Q}(\mathbf{u}_0) - \mathbf{Q}(\mathbf{u}_i)}_{\text{computed directly}} \tag{4.11}$$

Since in the GOAM process both $\mathbf{u}_0$ and $\tilde{\mathbf{u}}_i$ are computed, (4.11) *shows that to establish an accurate estimate of the modeling error in any multi-scale solution* $\mathbf{u}_i$*, it suffices to estimate the homogenization error* $\mathbf{Q}(\mathbf{u}) - \mathbf{Q}(\mathbf{u}_0)$.

This statement is part of the basic concept underlying the estimation process presented in this thesis work. In the following, the derivations focus on estimation of the homogenization error. Estimates of $\mathbf{Q}(\mathbf{u}) - \mathbf{Q}(\tilde{\mathbf{u}}_i)$ are subsequently established by applying (4.11).

The goal is to only employ local descriptions that are signifiicant in terms of the goals of the analyses. Thus, given a quantity of interest $\mathbf{Q}(\mathbf{u})$ that is defined on a small subdomain $\omega \subset \Omega$ (*e.g.* the examples in Section 3.2), the estimation process focuses on employing problem descriptions on ω only.

In Section 2.1 it is stated that the fine-scale solution satisfies the elastostatic PDE $(2.1)^1$ in Ω. Since $\omega \subset \Omega$, it must hold that

$$-\nabla \cdot \mathbf{E}\nabla\mathbf{u} = \mathbf{f} \quad \text{in } \omega \tag{4.12}$$

Multiplying (4.12) by an arbitrary test function $\mathbf{v} \in \mathbf{H}^1(\omega)$, integrating over ω, and subsequently applying Green's Identity, the following local

variational formulation is obtained:

$$\int_\omega \mathbf{E}\nabla\mathbf{u}\cdot\nabla\mathbf{v}\;\mathrm{d}\mathbf{x} = \int_\omega \mathbf{f}\cdot\mathbf{v}\;\mathrm{d}\mathbf{x} + \int_{\partial\omega}(\mathbf{E}\nabla\mathbf{u}^+\mathbf{n}_\omega)\cdot\mathbf{v}\;\mathrm{d}\mathbf{s} \quad \forall\mathbf{v}\in\mathbf{H}^1(\omega) \quad (4.13)$$

where $\mathbf{n}_\omega$ denotes the unit normal to the boundary $\partial\omega$ and $\mathbf{E}\nabla\mathbf{u}^+\mathbf{n}_\omega$ denotes the traction applied to $\partial\omega$ by the surrounding external stress field. For the purpose of this derivation, the latter is treated as an externally applied load.. By introducing the local bilinear and linear forms

$$\begin{aligned}\mathbf{B}_\omega(\mathbf{u},\mathbf{v}) &\stackrel{\text{def}}{=} \int_\omega \mathbf{E}\nabla\mathbf{u}\cdot\nabla\mathbf{v}\;\mathrm{d}\mathbf{x}\\ \mathbf{F}_\omega(\mathbf{v}) &\stackrel{\text{def}}{=} \int_\omega \mathbf{f}\cdot\mathbf{v}\;\mathrm{d}\mathbf{x} + \int_{\partial\omega}(\mathbf{E}\nabla\mathbf{u}^+\mathbf{n}_\omega)\cdot\mathbf{v}\;\mathrm{d}\mathbf{s}\end{aligned} \quad (4.14)$$

this allows (4.13) to be rewritten as

$$\mathbf{B}_\omega(\mathbf{u},\mathbf{v}) = \mathbf{F}_\omega(\mathbf{v}) \quad \forall\mathbf{v}\in\mathbf{H}^1(\omega) \quad (4.15)$$

Following the approach taken by Oden *et al* (see Section 4.1), seeking $\mathbf{u}$ in terms of $\mathbf{Q}(\mathbf{u})$ that satisfies (4.15) can equivalently be prescribed by the following constraint minimization problem:

$$\begin{aligned}\mathbf{Q}(\mathbf{u}) &= \inf_{\mathbf{v}\in\mathcal{M}}\mathbf{Q}(\mathbf{v})\\ \mathcal{M} &= \big\{\mathbf{v}\in\mathbf{H}^1(\omega) : \mathbf{B}_\omega(\mathbf{v},\mathbf{w}) - \mathbf{F}(\mathbf{w}) = 0, \quad \forall\mathbf{w}\in\mathbf{H}^1(\omega)\big\}\end{aligned} \quad (4.16)$$

As in Section 4.1, the solution of this contraint minimization problem is governed by the minizer/saddle point $(\mathbf{u},\mathbf{p})$ of the local Lagrangian:

$$\mathbf{L}_\omega(\mathbf{v},\mathbf{q}) = \mathbf{Q}(\mathbf{v}) + \mathbf{F}_\omega(\mathbf{q}) - \mathbf{B}_\omega(\mathbf{v},\mathbf{q}) \quad (4.17)$$

Then the roots of the Gateaux derivative of the Lagrangian, are given by:

$$\begin{aligned}\delta\mathbf{L}_\omega\Big((\mathbf{w},\mathbf{p}),(\mathbf{v},\mathbf{q})\Big) &= \lim_{\theta\to 0}\frac{1}{\theta}\Big[\mathbf{L}_\omega\big((\mathbf{w},\mathbf{p})+\theta(\mathbf{v},\mathbf{q})\big) - \mathbf{L}_\omega(\mathbf{w},\mathbf{p})\Big] = 0\\ &\forall(\mathbf{v},\mathbf{q})\in\mathbf{H}^1(\omega)\times\mathbf{H}^1(\omega)\end{aligned} \quad (4.18)$$

Again assuming linearity of $\mathbf{F}_\omega(\cdot)$, $\mathbf{B}_\omega(\cdot,\cdot)$, and $\mathbf{Q}(\cdot)$ simplifies (4.18) to:

$$\big[\mathbf{Q}(\mathbf{v}) - \mathbf{B}_\omega(\mathbf{v},\mathbf{p})\big] + \big[\mathbf{F}(\mathbf{q}) - \mathbf{B}_\omega(\mathbf{w},\mathbf{q})\big] = 0 \quad \forall (\mathbf{v},\mathbf{q}) \in \mathbf{H}^1(\omega) \times \mathbf{H}^1(\omega) \tag{4.19}$$

where $(\mathbf{v},\mathbf{q})$ denotes the pair of test functions.

Likewise, (4.19) is only satisfied if

$$\boxed{\begin{aligned} \mathbf{B}_\omega(\mathbf{w},\mathbf{q}) &= \mathbf{F}(\mathbf{q}) \quad \forall \mathbf{q} \in \mathbf{H}^1(\omega) \\ \mathbf{B}_\omega(\mathbf{v},\mathbf{p}) &= \mathbf{Q}(\mathbf{v}) \quad \forall \mathbf{v} \in \mathbf{H}^1(\omega) \end{aligned}} \tag{4.20}$$

where $(4.20)^1$ is known as the *local primal problem*, and $(4.20)^2$ is known as the *local dual problem*.

Proposition 4.2.1. *1. The solution* $\mathbf{p}$ *of the local dual problem* $(4.20)^2$ *exists if and only if the quantity of interest is continuous with respect to the seminorm* $\sqrt{\mathbf{B}_\omega(\cdot,\cdot)}$ *on* ω*, that is:*

$$\exists C > 0 : \qquad \mathbf{Q}(\mathbf{v}) \leq C\sqrt{\mathbf{B}_\omega(\mathbf{v},\mathbf{v})}, \qquad \forall \mathbf{v} \in H^1(\omega). \tag{4.21}$$

2. The solution $\mathbf{p}$ *is unique up to an unknown constant.*

Proof. Both assertions are established by invoking the Generalized Lax-Milgram Theorem. □

Due to the continuity requirement (4.21) on $\mathbf{Q}(\cdot)$, errors in linear quantities of interest involving displacement terms cannot be predicted using the dual problem $(4.20)^2$. These quantities of interest are continuous in terms of the $L^2(\omega)$ norm, but not in terms of the seminorm, meaning the solution

$\mathbf{p}$ does not exist. However, linear quantities of interest in terms of stresses and strains do satisfy the continuity requirement and lead to computable dual solutions and successful predictions of error.

Compared to the previously established error estimation process described in Section 4.1, the estimator described here distinguishes itself in two important ways:

1. *The dual problem* $(4.20)^2$ *is computable.* Unlike previous approaches, in which the dual problem was defined globally, the dual problem presented here is defined only on the domain of interest, a small subdomain $\omega \subset \Omega$, allowing it to contain the necessary fine-scale information in the domain of interest without requiring computationally prohibitive global integration. This allows $\mathbf{p}$ to be computed exactly and eliminates the loss of accuracy associated with the use of a surrogate dual problem.

2. *The dual problem only needs to be solved once.* This is directly related to the ability to solve the dual problem exactly. Since previous approaches cast the dual problem in terms of global integrals, it was only possible to approximate the dual problem by using some surrogate model. As a result, each successive enhancement of the surrogate model required an additional computation of the dual problem. With the local dual problem, the solution $\mathbf{p}$ does not depend on the surrogate model and only needs to be computed once, regardless of the number of adaptive iterations necessary to achieve the desired target error.

Having the definition of the local dual problem in place, one can immediately establish an assessment of the modeling error in the homogenized

solution $\mathbf{u}_0$.

Lemma 4.2.1. *Let* $\mathbf{u}$ *be the solution of the model problem* (2.1) *and* $\mathbf{p} \in \mathbf{H}^1(\omega)$ *be the solution of the local dual problem* (4.20)[2]*. Then, the following equality holds for the homogenization error in the quantity of interest:*

$$\mathbf{Q}(\mathbf{u}) - \mathbf{Q}(\mathbf{u}_0) = \int_\omega (\mathbf{E}_0 - \mathbf{E})\nabla \mathbf{u}_0 \cdot \nabla \mathbf{p} \; d\mathbf{x} + \int_{\partial\omega} (\mathbf{E}\nabla \mathbf{u} \mathbf{n}_\omega - \mathbf{E}_0 \nabla \mathbf{u}_0 n_\omega) : \mathbf{p} \; d\mathbf{s} \tag{4.22}$$

Proof. Choosing $\mathbf{p}$ for the test function $\mathbf{v}$ of the dual problem, one obtains

$$\mathbf{Q}(\mathbf{u}) - \mathbf{Q}(\mathbf{u}_0) = \mathbf{B}_\omega(\mathbf{u}, \mathbf{p}) - \mathbf{B}_\omega(\mathbf{u}_0, \mathbf{p})$$

Substitution of the local primal problem (4.15) yields:

$$\begin{aligned}
\mathbf{Q}(\mathbf{u}) - \mathbf{Q}(\mathbf{u}_0) &= \mathbf{F}_\omega(\mathbf{p}) - \mathbf{B}_\omega(\mathbf{u}_0, \mathbf{p}) \\
&= \int_\omega \mathbf{f} \cdot \mathbf{p} \; \mathrm{d}\mathbf{x} + \int_{\partial\omega} (\mathbf{E}\nabla \mathbf{u} \mathbf{n}_\omega) \cdot \mathbf{p} \; \mathrm{d}\mathbf{s} \\
&\qquad - \int_\omega \mathbf{E}\nabla \mathbf{u}_0 \cdot \nabla \mathbf{p} \; \mathrm{d}\mathbf{x} \\
&= \underbrace{\int_\omega \mathbf{f} \cdot \mathbf{p} \; \mathrm{d}\mathbf{x} + \int_{\partial\omega} (\mathbf{E}_0 \nabla \mathbf{u}_0 \mathbf{n}_\omega) \cdot \mathbf{p} \; \mathrm{d}\mathbf{s}} \\
&\qquad - \int_{\partial\omega} (\mathbf{E}_0 \nabla \mathbf{u}_0 \mathbf{n}_\omega) \cdot \mathbf{p} \; \mathrm{d}\mathbf{s} + \int_{\partial\omega} (\mathbf{E}\nabla \mathbf{u} \mathbf{n}_\omega) \cdot \mathbf{p} \; \mathrm{d}\mathbf{s} \\
&\qquad - \int_\omega \mathbf{E}\nabla \mathbf{u}_0 \cdot \nabla \mathbf{p} \; \mathrm{d}\mathbf{x}
\end{aligned}$$

Considering the homogenized surrogate PDE,

$$-\nabla \cdot (\mathbf{E}_0 \nabla \mathbf{u}_0) = \mathbf{f}, \quad \text{in } \omega \tag{4.23}$$

and its equivalent variational form,

$$\int_\omega \mathbf{E}_0 \nabla \mathbf{u}_0 \cdot \nabla \mathbf{p} \, \mathrm{d}\mathbf{x} = \int_\omega \mathbf{f} \cdot \mathbf{p} \, \mathrm{d}\mathbf{x} + \int_{\partial\omega} (\mathbf{E}_0 \nabla \mathbf{u}_0 \mathbf{n}_\omega) \cdot \mathbf{p} \, \mathrm{d}\mathbf{s} \tag{4.24}$$

reveals that the collected term may be rewritten, giving:

$$\mathbf{Q}(\mathbf{u}) - \mathbf{Q}(\mathbf{u}_0) = \int_\omega \mathbf{E}_0 \nabla \mathbf{u}_0 \cdot \nabla \mathbf{p} \, \mathrm{d}\mathbf{x} + \int_{\partial\omega} (\mathbf{E} \nabla \mathbf{u} \mathbf{n}_\omega - \mathbf{E}_0 \nabla \mathbf{u}_0 \mathbf{n}_\omega) \cdot \mathbf{p} \, \mathrm{d}\mathbf{s}$$

□

Remark 4.2.1. It is important to note that even though $\mathbf{p}$ is unique up to an arbitrary constant, this degree of freedom does not affect the prediction of the homogenization error (4.22). This can be illustrated by considering $\mathbf{p} + \mathbf{C}$, where $\mathbf{C}$ is an arbitrary constant function:

$$\begin{aligned}
\mathbf{Q}(\mathbf{u}) - \mathbf{Q}(\mathbf{u}_0) &= \int_\omega (\mathbf{E}_0 - \mathbf{E}) \nabla \mathbf{u}_0 : \nabla (\mathbf{p} + \mathbf{C}) \mathrm{d}\mathbf{x} \\
&\quad + \int_{\partial\omega} [\mathbf{E} \nabla \mathbf{u} \mathbf{n}_\omega - \mathbf{E}_0 \nabla \mathbf{u}_0 \mathbf{n}_\omega] : (\mathbf{p} + \mathbf{C}) \mathrm{d}s \\
&= \int_\omega (\mathbf{E}_0 - \mathbf{E}) \nabla \mathbf{u}_0 : \nabla \mathbf{p} \mathrm{d}\mathbf{x} + \int_{\partial\omega} [\mathbf{E} \nabla \mathbf{u} \mathbf{n}_\omega - \mathbf{E}_0 \nabla \mathbf{u}_0 \mathbf{n}_\omega] : \mathbf{p} \mathrm{d}s \\
&\quad + \int_{\partial\omega} [\mathbf{E} \nabla \mathbf{u} \mathbf{n}_\omega - \mathbf{E}_0 \nabla \mathbf{u}_0 \mathbf{n}_\omega] : \mathbf{C} \mathrm{d}s
\end{aligned}$$

Noting, however, by (4.15) and (4.24) that the last term is identically equal to zero then reduces the equation to (4.22).

The expression (4.22) is still not computable, as the traction $\mathbf{E} \nabla \mathbf{u} \mathbf{n}_\omega$ depends on the surrounding fine-scale solution $\mathbf{u}$, which is generally unsolvable. The estimation of this term is based on the following observation:

Note that the exact and homogenized solutions satisfy PDEs (4.12) and (4.23) in Ω. Hence, they must also satisfy these equations in the subdomain

$\omega \subset \Omega$

$$\begin{aligned} -\nabla \cdot (\mathbf{E}\nabla \mathbf{u}) &= \mathbf{f}, \quad \text{in } \omega \\ -\nabla \cdot (\mathbf{E}_0 \nabla \mathbf{u}_0) &= \mathbf{f}, \quad \text{in } \omega \end{aligned}$$

Hence,

$$-\nabla \cdot (\mathbf{E}\nabla \mathbf{u}) = -\nabla \cdot (\mathbf{E}_0 \nabla \mathbf{u}_0) \quad \text{in } \omega$$

and therefore,

$$-\int_\omega \nabla \cdot (\mathbf{E}\nabla \mathbf{u}) \, \mathrm{d}\mathbf{x} = -\int_\omega \nabla \cdot (\mathbf{E}_0 \nabla \mathbf{u}_0) \, \mathrm{d}\mathbf{x}$$

Applying the Gauss divergence theorem then yields

$$\int_{\partial\omega} (\mathbf{E}\nabla \mathbf{u}\mathbf{n}_\omega) \, \mathrm{d}\mathbf{s} = \int_{\partial\omega} (\mathbf{E}_0 \nabla \mathbf{u}_0 \mathbf{n}_\omega) \, \mathrm{d}\mathbf{s}$$

Thus, in the *average sense*, the traction of the homogenized solution is identical to that of the fine-scale solution.

*Therefore, it is proposed that in order to estimate the homogenization error after the first step in the GOAM process, (*i.e. *after the homogenized solution has been computed), the term* $\mathbf{E}\nabla \mathbf{u}\mathbf{n}_\omega$ *in* (4.22) *may be estimated by* $\mathbf{E}_0 \nabla \mathbf{u}_0 \mathbf{n}_\omega$*, and the following estimate is proposed:*

$$\boxed{\mathbf{Q}(\mathbf{u}) - \mathbf{Q}(\mathbf{u}_0) \approx \eta_0 = \int_\omega (\mathbf{E}_0 - \mathbf{E}) \nabla \mathbf{u}_0 \cdot \nabla \mathbf{p} \, \mathrm{d}\mathbf{x}} \tag{4.25}$$

Numerical verifications of this error estimate are provided in Section 5.1 and show that reasonable to good accuracy in estimating $\mathbf{Q}(\mathbf{u}) - \mathbf{Q}(\mathbf{u}_0)$ is established.

To estimate the error of subsequent enhanced solutions $\tilde{\mathbf{u}}_i$, the estimate η_0 could be used in conjunction with (4.11), i.e.

$$\mathbf{Q}(\mathbf{u}) - \mathbf{Q}(\tilde{\mathbf{u}}_i) \approx \eta_0 + \mathbf{Q}(\mathbf{u}_0) - \mathbf{Q}(\tilde{\mathbf{u}}_i) \tag{4.26}$$

and numerical verifications of this estimate are shown in Section 5.1 as well. However, as the accuracy of solutions $\tilde{\mathbf{u}}_i$ increase with each enhancement, the inaccuracy in η_0 eventually renders the estimate in (4.26) of less practical use in later enhancement steps. It is preferable to use the additional information obtained with the enhanced solution in the estimation process, *i.e.* use the enhanced solution to obtain more accurate estimates of $\mathbf{Q}(\mathbf{u}) - \mathbf{Q}(\mathbf{u}_0)$, and accordingly by (4.11), of $\mathbf{Q}(\mathbf{u}) - \mathbf{Q}(\tilde{\mathbf{u}}_i)$ as well. The following enhanced estimate of $\mathbf{Q}(\mathbf{u}) - \mathbf{Q}(\mathbf{u}_0)$ is investigated in Section 5.1:

$$\eta_{avg} = \frac{1}{2}\big(\eta_0 + \mathbf{Q}(\tilde{\mathbf{u}}_1) - \mathbf{Q}(\mathbf{u}_0)\big) \tag{4.27}$$

Chapter 5

Numerical Verifications

In this chapter, the effectivity and accuracy of the goal-oriented error estimator (4.25) is verified. In Section 5.1, the results for a deterministic model are presented, and in Section 5.2, the results are presented of a preliminary investigation into the extension of the estimation process to stochastic problems.

5.1 Verification of Modeling Error Estimates

Consider a two-dimensional, heterogeneous rectangular beam as illustrated in Figure 5.1. The beam has prescribed tractions $\mathbf{t}_1 = 150$ MPa and $\mathbf{t}_2 = 50$ MPa and prescribed zero displacements along the edge $x = 0$. The beam is comprised of a two-phase composite material whose constituents are both linearly elastic and isotropic. The circular inclusions, with Young's Modulus and Poisson Ratio $E_{inc} = 150$ GPa and $\nu_{inc} = 0.2$, have been randomly interspersed throughout the matrix material, with Young's Modulus and Poisson Ratio $E_m = 4$ GPa and $\nu_m = 0.3$, with a volume fraction of 0.258.

For this test problem, the global domain Ω is divided into a regular grid of similar subdomains, $\omega_k, \quad k = 1, 2, \cdots, 88$, as illustrated in Figure 5.2, on which the following quantities of interest are chosen:

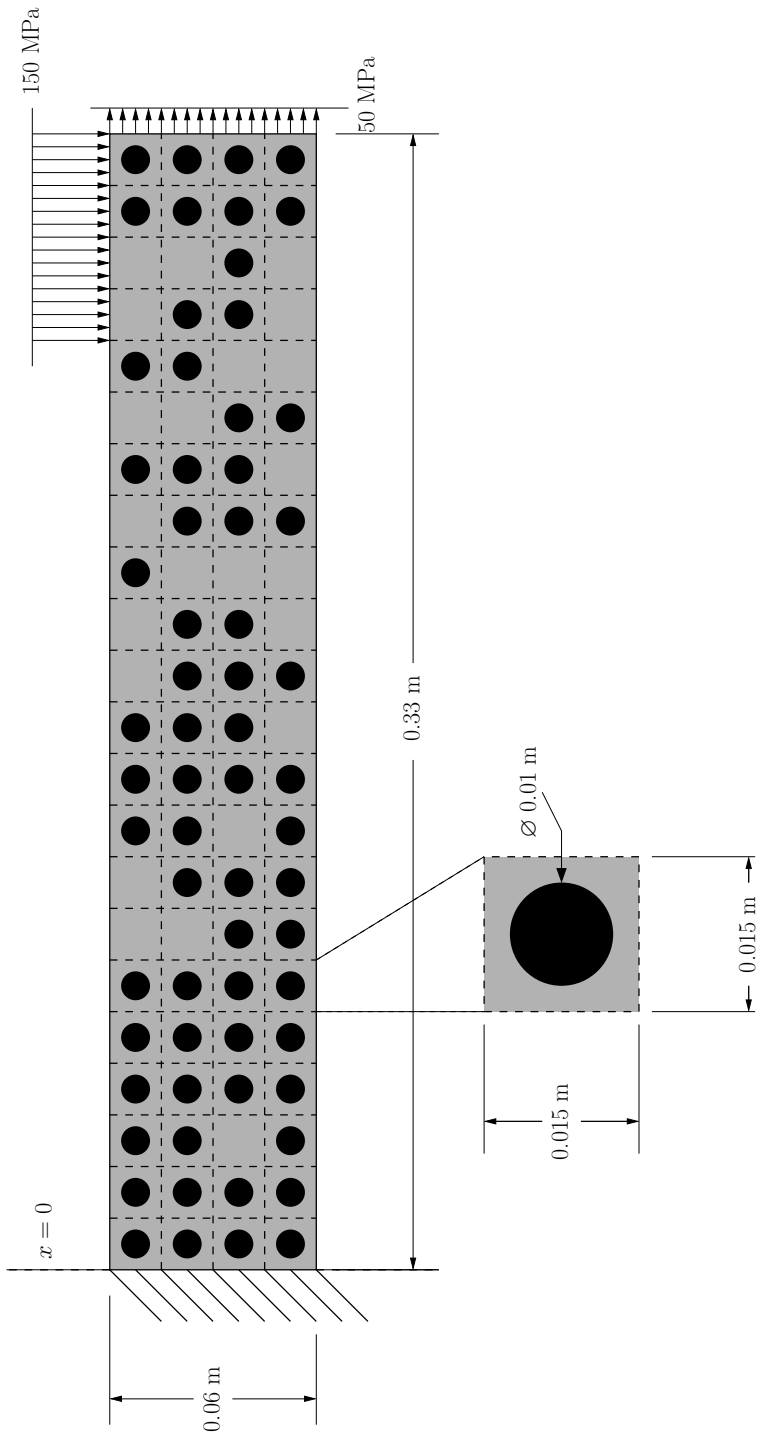

Figure 5.1: Test problem: a carbon-epoxy composite beam

Figure 5.2: Subdomain labels and enhancement regions for the test problem

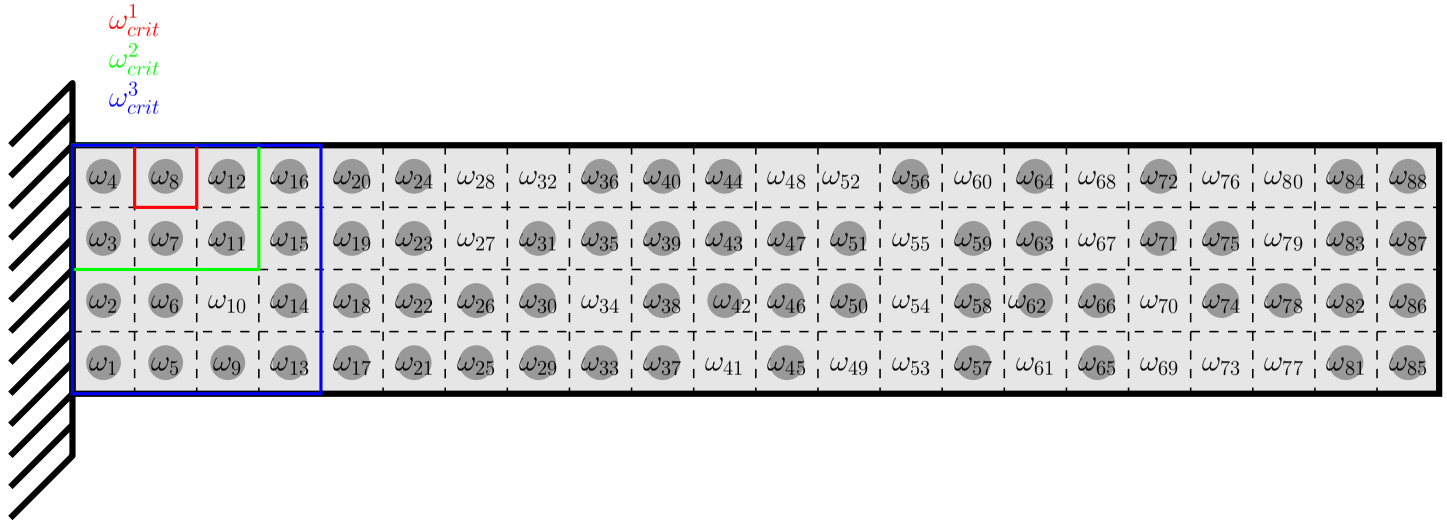

1. The average axial strain ε_{xx}:

$$\mathbf{Q}_i^x(\mathbf{u}) = \frac{1}{|\omega_i|}\int_{\omega_i} \varepsilon_{xx}(\mathbf{u})\mathrm{d}\mathbf{x} = \frac{1}{|\omega_i|}\int_{\omega_i} \frac{\partial u_x}{\partial x}\mathrm{d}\mathbf{x}$$

2. The average axial strain ε_{yy}:

$$\mathbf{Q}_i^y(\mathbf{u}) = \frac{1}{|\omega_i|}\int_{\omega_i} \varepsilon_{yy}(\mathbf{u})\mathrm{d}\mathbf{x} = \frac{1}{|\omega_i|}\int_{\omega_i} \frac{\partial u_y}{\partial y}\mathrm{d}\mathbf{x}$$

3. The average (engineering) shear strain γ_{xy}:

$$\mathbf{Q}_i^\gamma(\mathbf{u}) = \frac{1}{|\omega_i|}\int_{\omega_i} \gamma_{xy}(\mathbf{u})\mathrm{d}\mathbf{x} = \frac{1}{|\omega_i|}\int_{\omega_i} \left(\frac{\partial u_x}{\partial y} + \frac{\partial u_y}{\partial x}\right)\mathrm{d}\mathbf{x}$$

An overkill finite element approximation (see Figure 5.3 for the finite element mesh) of the exact solution $\mathbf{u}(\mathbf{x})$ is computed, with negligible numerical approximation error, the results of which are presented in Figure 5.4. Likewise, a similar approximation of the homogenized solution (see Appendix 1) is computed with the same mesh and solution parameters as the exact problem, with results in Figure 5.5.

Additionally, for each of the 88 domains of interest, a series of three enhanced problems are calculated with the same mesh and parameters using the global enhancement method as defined in Section 3.3.2: the first containing enhanced data only in the subdomain on which the quantity of interest is defined (ω_Q), the second adding enhanced data on the immediately adjacent subdomains, and the third adding enhanced data up to two subdomains from ω_Q in the $+x$ and $-x$ directions over the full height of the beam. The progressive growth of the enhanced region is illustrated for $\omega_Q = \omega_8$ by the colored lines in Figure 5.2, and plots of the solution fields are shown in Figures 5.6, 5.7, and 5.8.

Figure 5.3: Full finite element mesh

Figure 5.4: Contour plots of the exact strain fields

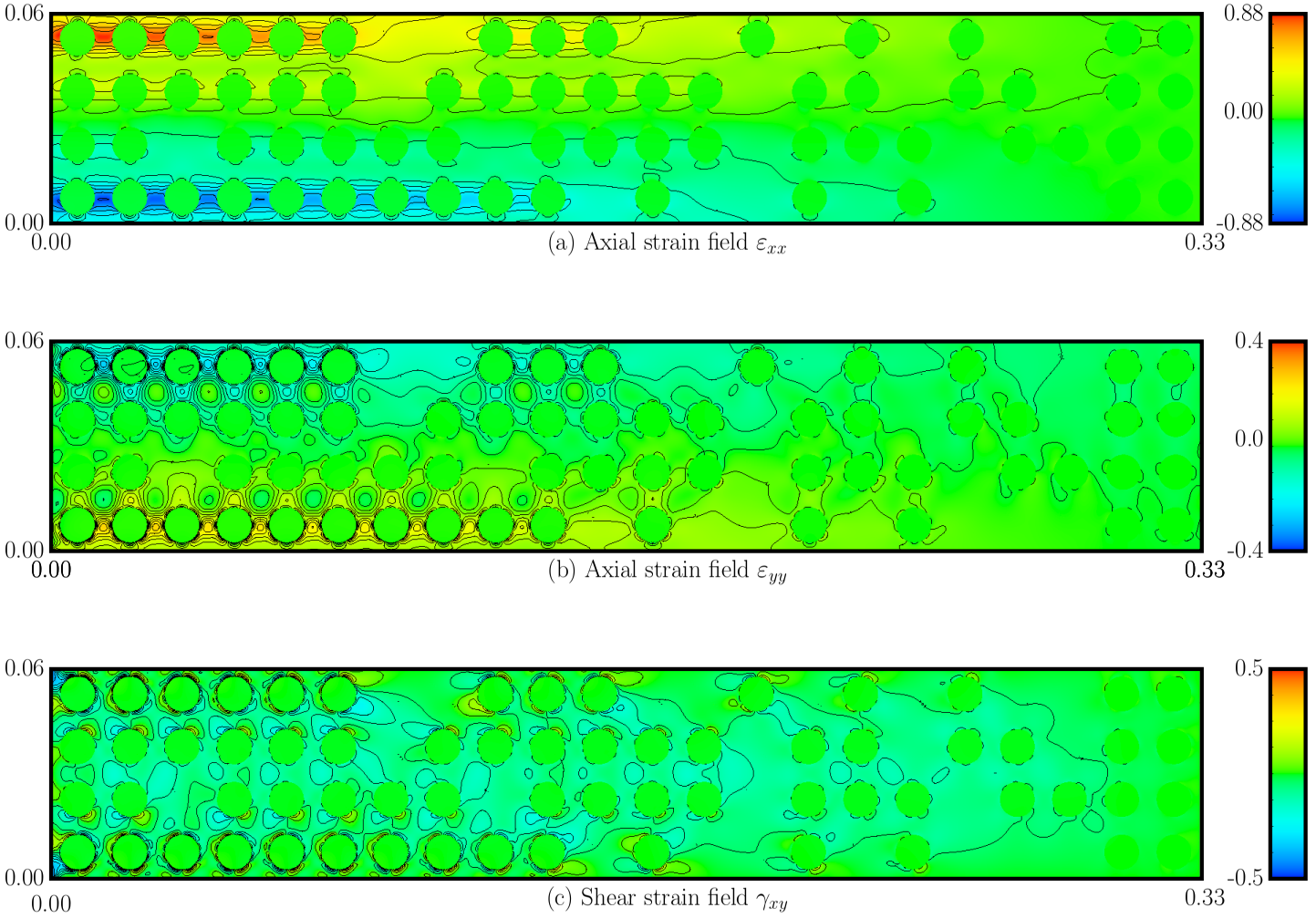

(a) Axial strain field ε_{xx}

(b) Axial strain field ε_{yy}

(c) Shear strain field γ_{xy}

Figure 5.5: Contour plots of the homogenized strain fields

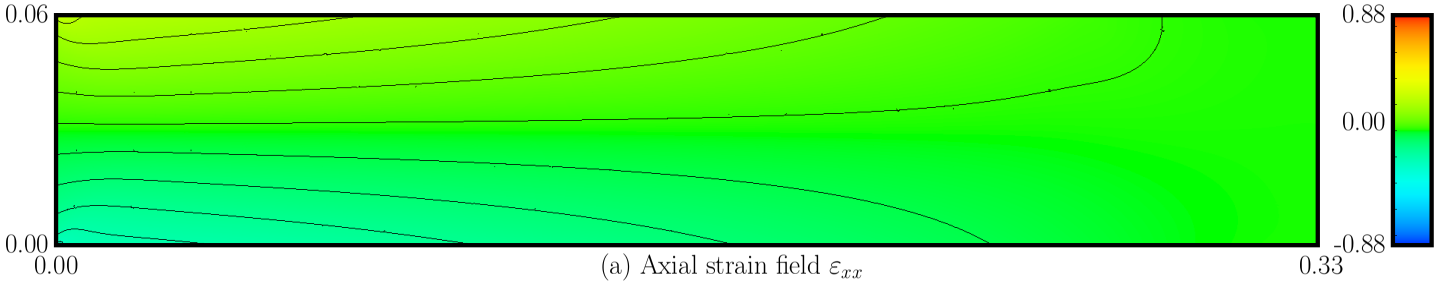

(a) Axial strain field ε_{xx}

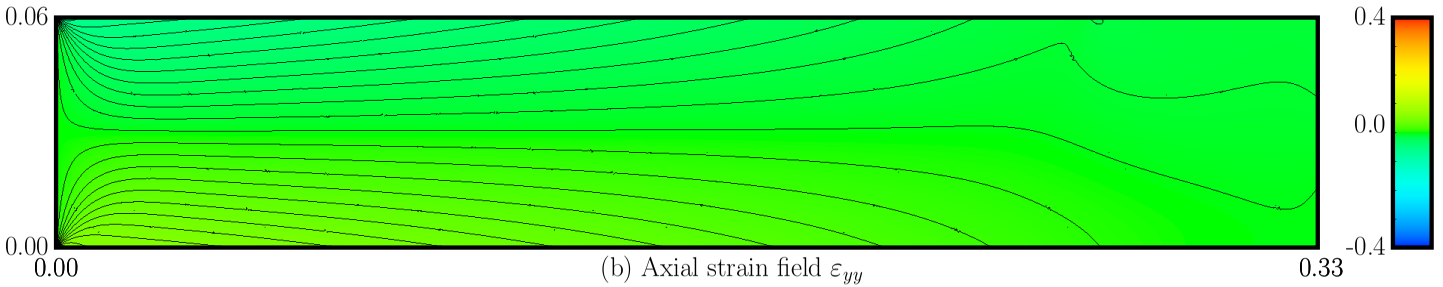

(b) Axial strain field ε_{yy}

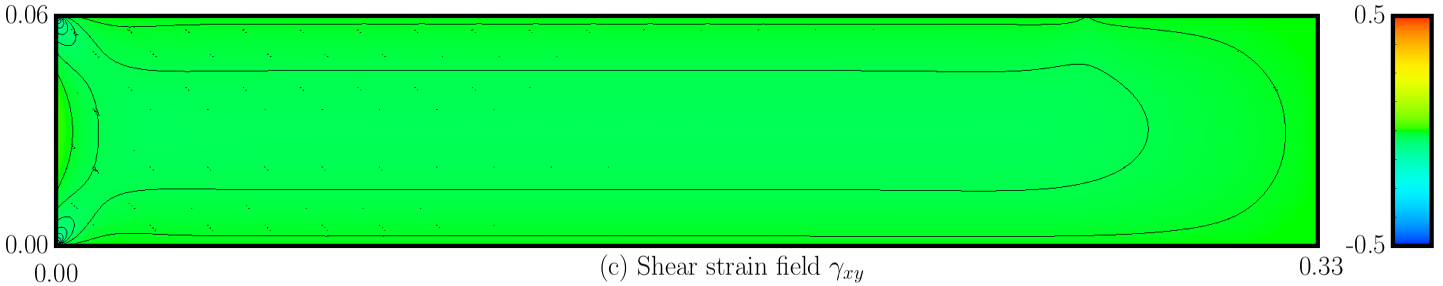

(c) Shear strain field γ_{xy}

Figure 5.6: Contour plots of the strain fields after the first enhancement

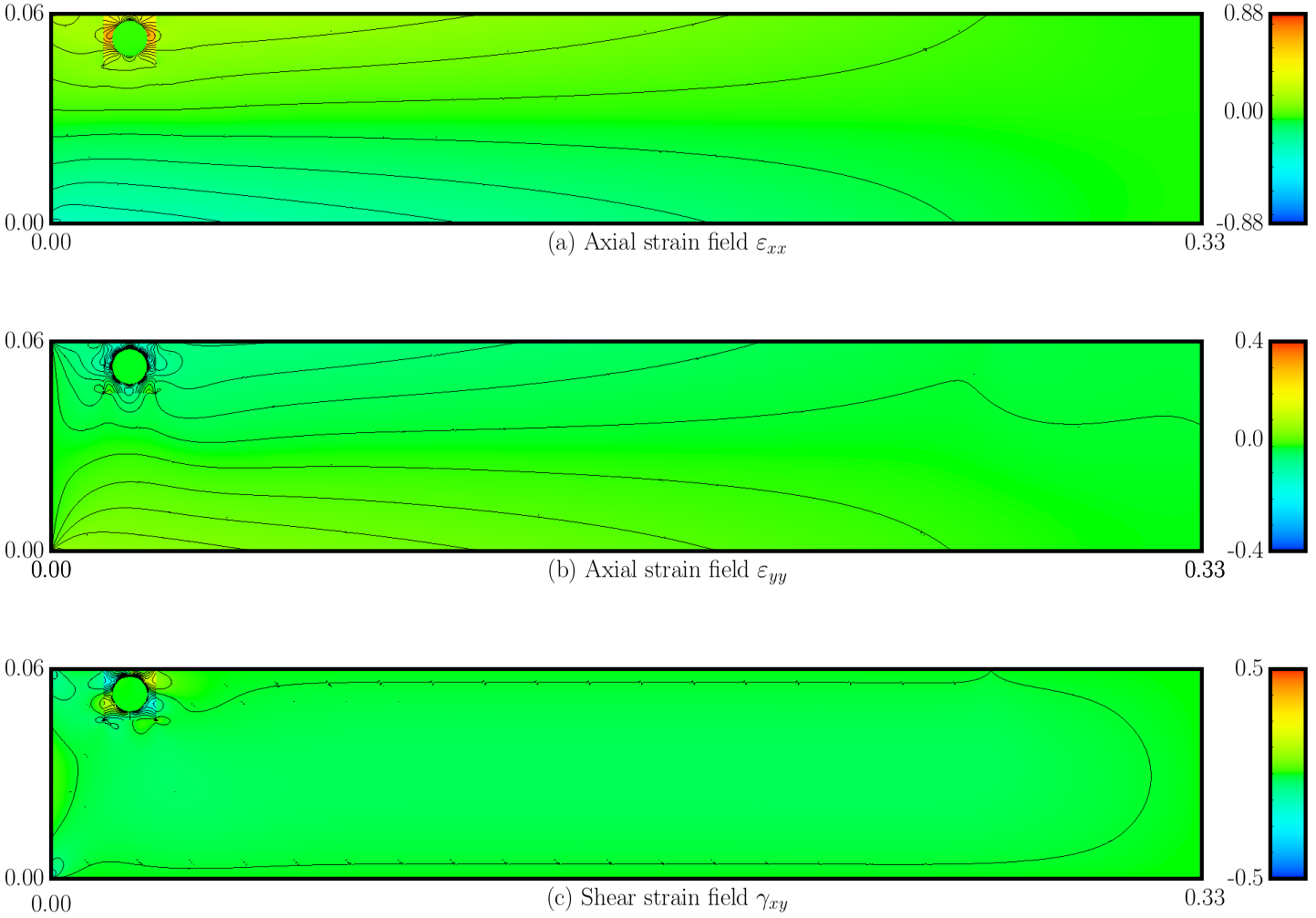

(a) Axial strain field ε_{xx}

(b) Axial strain field ε_{yy}

(c) Shear strain field γ_{xy}

Figure 5.7: Contour plots of the strain fields after the second enhancement

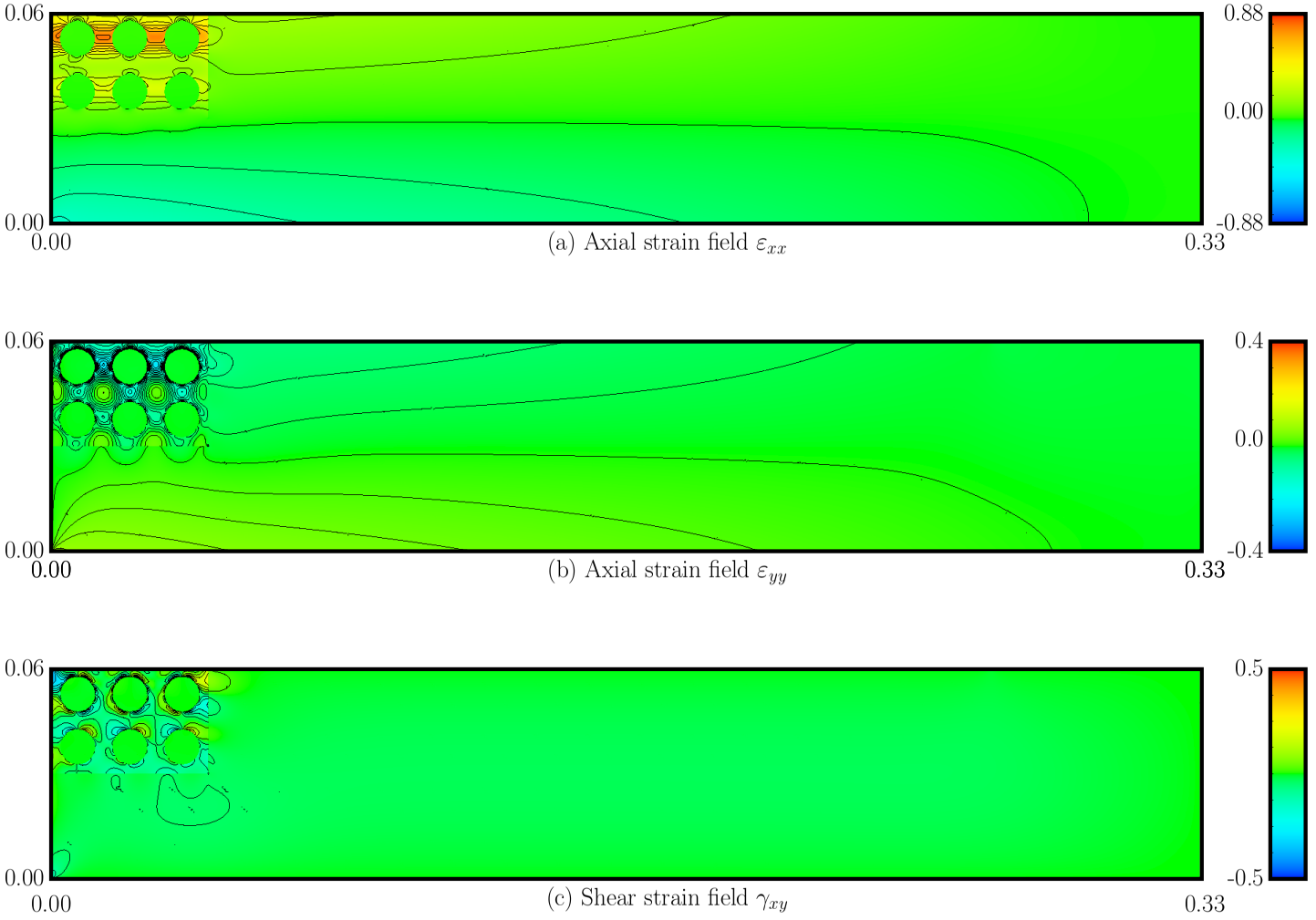

Figure 5.8: Contour plots of the strain fields after the third enhancement

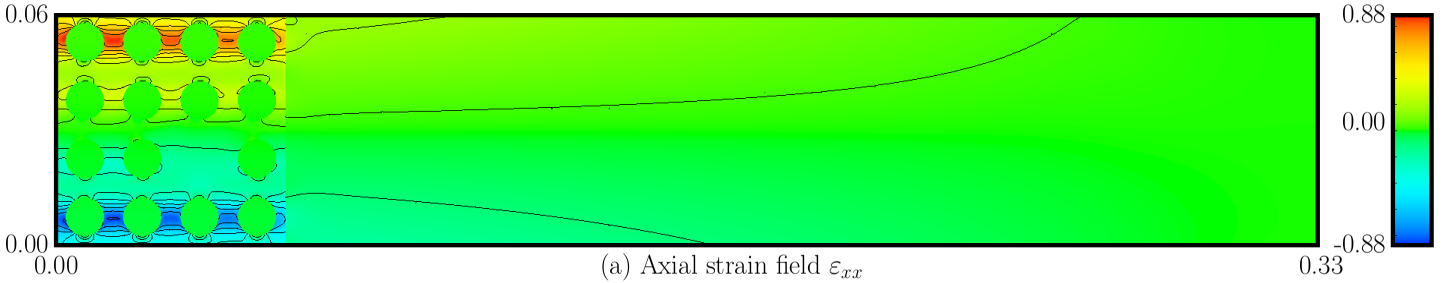

(a) Axial strain field ε_{xx}

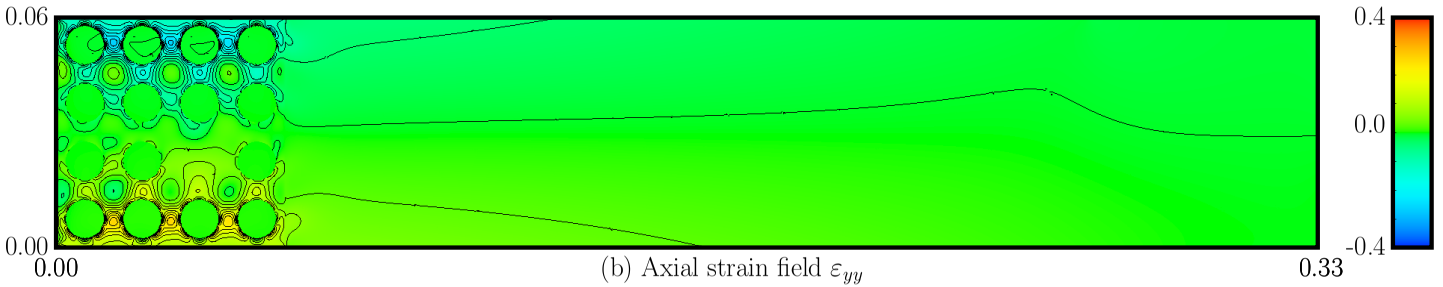

(b) Axial strain field ε_{yy}

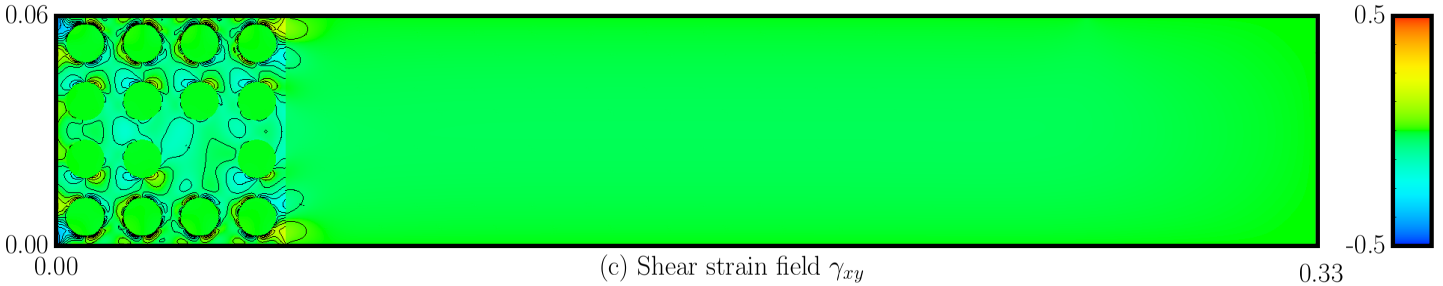

(c) Shear strain field γ_{xy}

As is clear in the solution of the exact problem, the presence of the stiff inclusions induces large strain gradients, with high strain concentrations in the matrix material immediately adjacent to the inclusions near the fixed end of the beam. The homogenized solution, of course, does not exhibit any such features and has a smooth strain field throughout the domain, with no concentrations or large gradients. The enhanced solutions display similar behavior to the exact solution in the regions where the exact material properties are provided.

Because the dual problem is local and independent of the location of physical space, and because there are only two types of subdomains: those with an inclusion and those without, *only six different dual problems need to be computed: one for each quantity of interest and subdomain type combination.* Because the dual solution is unique up to an unknown constant, a single point needs to be fixed for computation to proceed. No further boundary conditions need to be applied to $\partial\omega$. These dual problems are accordingly computed using the same numerical solution parameters used (*i.e.* mesh size and p-level) for the homogenized, exact, and enhanced problems (see Figure 5.9 for the finite element mesh), and their solutions are shown in Figures 5.10, 5.11, 5.12, 5.13, 5.14 and 5.15.

For this document, only the results for subdomains ω_1 through ω_{16} were tabulated, as the region formed by the union of these subdomains presents the highest strain gradients and concentrations and thus would be of primary interest to the analyst.

Using the solutions described above, the aforementioned quantities of

Figure 5.9: Finite element mesh for the dual problem

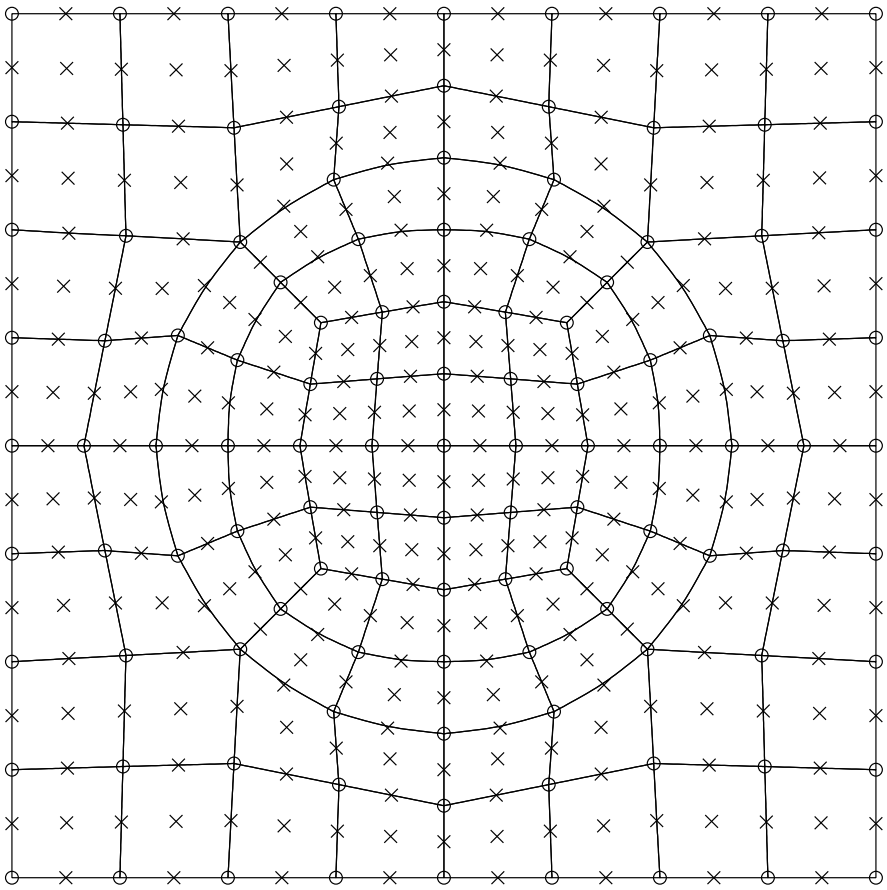

Figure 5.10: Contour plots of dual solution – quantity of interest is local average strain ε_{xx} with an inclusion

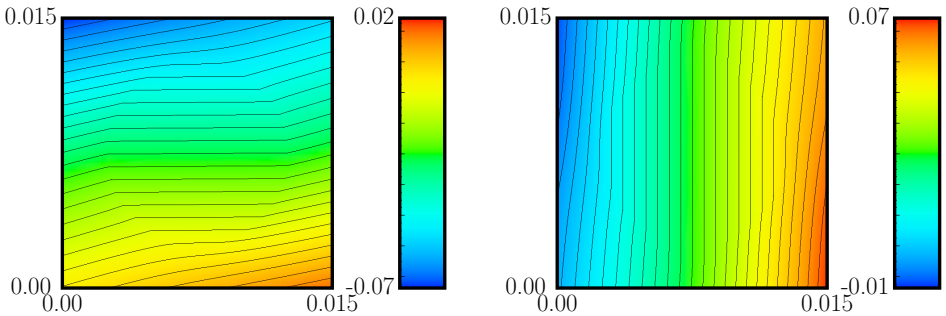

(a) Dual solution component p_x (b) Dual solution component p_y

Figure 5.11: Contour plots of dual solution – quantity of interest is local average strain ε_{xx} without an inclusion

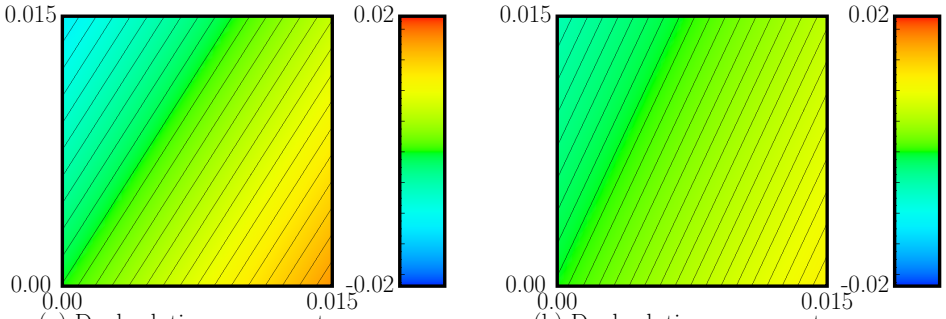

(a) Dual solution component p_x (b) Dual solution component p_y

Figure 5.12: Contour plots of dual solution – quantity of interest is local average strain ε_{yy} with an inclusion

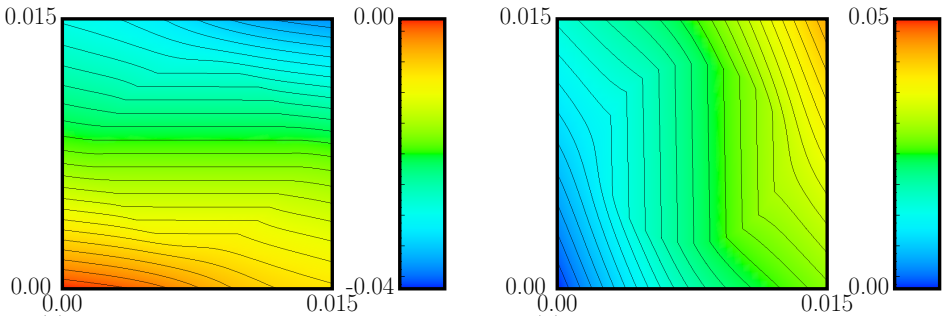

(a) Dual solution component p_x (b) Dual solution component p_y

Figure 5.13: Contour plots of dual solution – quantity of interest is local average strain ε_{yy} without an inclusion

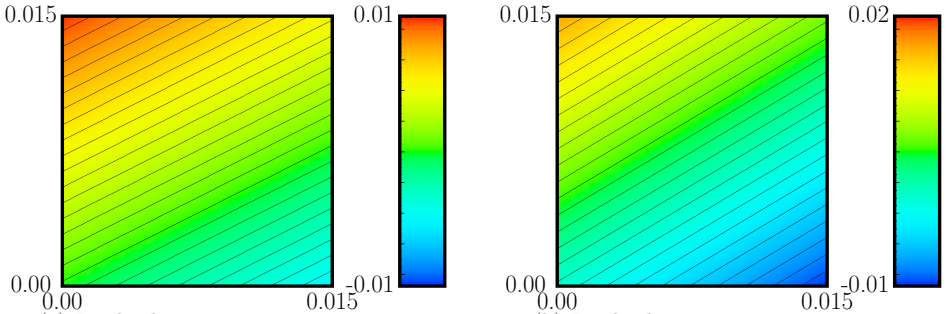

(a) Dual solution component p_x (b) Dual solution component p_y

Figure 5.14: Contour plots of dual solution – quantity of interest is local average strain γ_{xy} with an inclusion

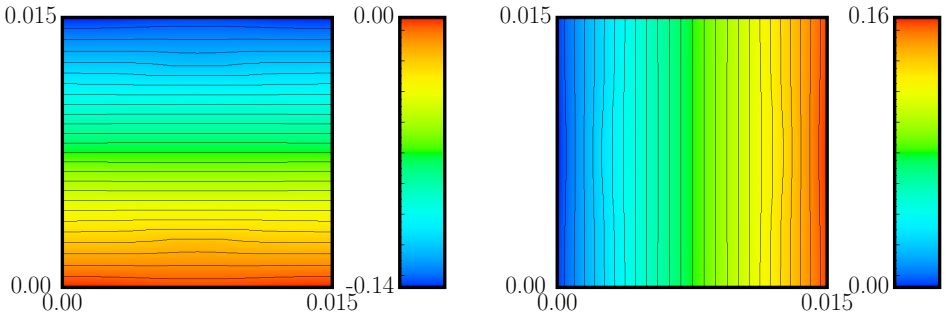

(a) Dual solution component p_x (b) Dual solution component p_y

Figure 5.15: Contour plots of dual solution – quantity of interest is local average strain γ_{xy} without an inclusion

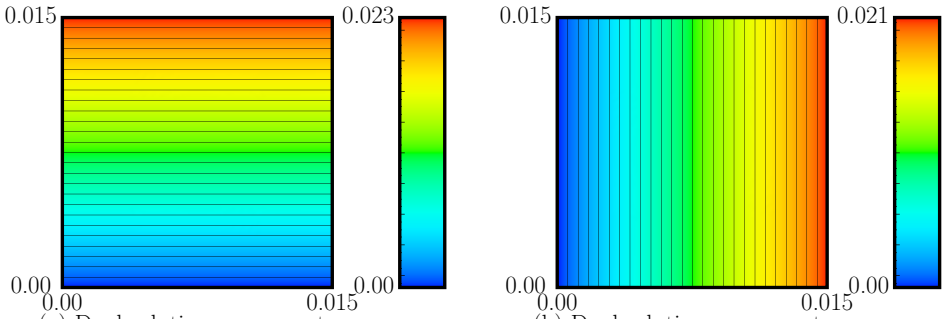

(a) Dual solution component p_x (b) Dual solution component p_y

interest are calculated for all of the defined subdomains for the homogenized, the exact, and the three enhanced solutions. The values of the quantities of interest are presented in Tables 5.1, 5.2, and 5.3. From these tables, two important conclusions are immediately apparent:

1. In all cases, the quantity of interest of the homogenized solution represents a poor approximation of the exact quantity of interest sought. Successive enhancements, however, improve the approximation rapidly.

2. The values of the quantity of interest $\mathbf{Q}^x(\cdot)$ are a full order of magnitude higher than those of the other two quantities $\mathbf{Q}^y(\cdot)$ and $\mathbf{Q}^\gamma(\cdot)$. This indicates that, for the analyst, $\mathbf{Q}^x(\cdot)$ is the most critical quantity to be studied.

The errors in the quantity of interest—that is, the quantities to be estimated—are presented, both in absolute and in relative form, in Tables 5.4, 5.5, 5.6, 5.7, 5.8, and 5.9. As is clear from these tables, the error in the quantity of interest generally diminishes rapidly with each successive enhancement, and by the third enhancement, the errors in the quantities of interest are nearly zero. Since effectivity indices of error enhancements involve division by the error, an error near zero will cause effectivity indices associated with that error to appear poor. For the third enhancement, the error is on the order of 10^{-5}. Because of this, estimates and their effectivity indices will not be presented for the third enhancement.

Two different estimates of the error are investigated. First, the estima-

tor derived in Section 4.2 and presented in (4.25),

$$\begin{aligned} \mathbf{Q}(\mathbf{u}) - \mathbf{Q}(\mathbf{u}_0) \approx \eta_0 &= \int_\omega (\mathbf{E}_0 - \mathbf{E}) \nabla \mathbf{u}_0 \cdot \nabla \mathbf{p} \, \mathrm{d}\mathbf{x} \\ \mathbf{Q}(\mathbf{u}) - \mathbf{Q}(\tilde{\mathbf{u}}_\mathbf{i}) \approx \eta_{0,i} &= \eta_0 + \mathbf{Q}(\mathbf{u}_0) - \mathbf{Q}(\tilde{\mathbf{u}}_i) \end{aligned}$$

The results of these estimates are tabulated in Tables 5.10, 5.11, and 5.12 for homogenization and enhancement error estimates based on η_0, and in Table 5.13 for the error estimates based on η_{avg}.

As is clear from these tables, the estimates based on η_0 provide good estimates of the error for the homogenized and first enhancement solutions, but the performance for the central subdomains for the second enhancement is poor, even of the wrong sign in some cases, as the error in this setting is of the same order as the inaccuracy in η_0. It is noteworthy, however, that even though effectivity indices are generally unsatisfactory for $\eta_{0,2}$, the error estimates themselves still follow the same trend as the error, *i.e.* when the error diminishes from one enhancement to the next, even by a large amount, the estimate does as well. It is also worthwhile to note that the degradation of the estimate is most pronounced for $\mathbf{Q}^y(\cdot)$, where errors are relatively small to begin with, and that for the quantity of particular interest to the analyst ($\mathbf{Q}^x(\cdot)$), the estimate only experiences serious degradation along the central two rows of the domain, where strains are small to begin with, and remains reasonably good on the upper and lower rows of subdomains, where most bending strains take place. Nevertheless, some way of improving this estimate is needed to estimate the error for enhanced solutions.

As an initial attempt to improve this estimate, a second estimate, η_{avg}

is numerically explored, defined as:

$$\begin{aligned}\mathbf{Q}(\mathbf{u}) - \mathbf{Q}(\mathbf{u}_0) \approx \eta_{avg} &= \frac{1}{2}\big(\eta_0 + \mathbf{Q}(\tilde{\mathbf{u}}_1) - \mathbf{Q}(\mathbf{u}_0)\big) \\ \mathbf{Q}(\mathbf{u}) - \mathbf{Q}(\tilde{\mathbf{u}}_\mathbf{i}) \approx \eta_{avg,i} &= \eta_{avg} + \mathbf{Q}(\mathbf{u}_0) - \mathbf{Q}(\tilde{\mathbf{u}}_i)\end{aligned}$$

It is important to note that this estimate is proposed based on numerical results obtained from the η_0-based estimates. There is no rigorous theoretical background upon which this estimate is based. As such, this estimate is only explored for $\mathbf{Q}^x(\cdot)$. The results of this estimate are tabulated in Table 5.13.

As can be seen from this table,the improvement in this estimate is drastic, with effectivity indices close to unity, even for many estimates of the error in the second enhancement. Additionally, the estimates remain the same sign as the error, even in regions of low error, and where the actual error itself changes sign. Despite this marked improvement, it still important to note that there is no rigorous theoretical basis for this estimate, and estimation of error for the enhanced problems remains an open issue.

Table 5.1: Quantity of interest $\mathbf{Q}^x(\mathbf{u})$ for a deterministic problem, applying three enhancements

i	$\mathbf{Q}_i^x(\mathbf{u})$	$\mathbf{Q}_i^x(\mathbf{u}_0)$	$\mathbf{Q}_i^x(\mathbf{u}_1)$	$\mathbf{Q}_i^x(\mathbf{u}_2)$	$\mathbf{Q}_i^x(\mathbf{u}_3)$
1	-2.866e-01	-1.644e-01	-2.452e-01	-2.571e-01	-2.865e-01
2	-8.099e-02	-4.941e-02	-6.326e-02	-9.581e-02	-8.121e-02
3	9.703e-02	5.672e-02	7.260e-02	1.078e-01	9.722e-02
4	2.960e-01	1.722e-01	2.567e-01	2.703e-01	2.960e-01
5	-2.837e-01	-1.584e-01	-2.442e-01	-2.576e-01	-2.838e-01
6	-8.019e-02	-5.065e-02	-6.871e-02	-8.928e-02	-8.028e-02
7	9.728e-02	5.847e-02	7.929e-02	1.090e-01	9.751e-02
8	2.901e-01	1.661e-01	2.559e-01	2.642e-01	2.900e-01
9	-2.724e-01	-1.497e-01	-2.323e-01	-2.508e-01	-2.722e-01
10	-1.288e-01	-4.753e-02	-9.098e-02	-1.389e-01	-1.298e-01
11	9.091e-02	5.542e-02	7.566e-02	1.014e-01	9.076e-02
12	2.753e-01	1.574e-01	2.441e-01	2.532e-01	2.755e-01
13	-2.541e-01	-1.409e-01	-2.190e-01	-2.331e-01	-2.531e-01
14	-6.890e-02	-4.440e-02	-6.067e-02	-7.592e-02	-7.074e-02
15	8.949e-02	5.225e-02	7.136e-02	9.607e-02	8.856e-02
16	2.574e-01	1.487e-01	2.308e-01	2.397e-01	2.584e-01

Table 5.2: Quantity of interest $\mathbf{Q}^y(\mathbf{u})$ for a deterministic problem, applying three enhancements

i	$\mathbf{Q}_i^y(\mathbf{u})$	$\mathbf{Q}_i^y(\mathbf{u}_0)$	$\mathbf{Q}_i^y(\mathbf{u}_1)$	$\mathbf{Q}_i^y(\mathbf{u}_2)$	$\mathbf{Q}_i^y(\mathbf{u}_3)$
1	5.667e-02	3.303e-02	3.884e-02	4.991e-02	5.670e-02
2	1.034e-02	7.010e-03	6.400e-03	1.132e-02	1.040e-02
3	-1.245e-02	-7.797e-03	-6.997e-03	-1.258e-02	-1.264e-02
4	-5.818e-02	-3.441e-02	-4.047e-02	-5.224e-02	-5.827e-02
5	8.030e-02	4.198e-02	4.858e-02	7.191e-02	8.042e-02
6	2.100e-02	1.310e-02	1.640e-02	1.957e-02	2.122e-02
7	-2.223e-02	-1.491e-02	-1.860e-02	-2.278e-02	-2.231e-02
8	-8.020e-02	-4.395e-02	-5.091e-02	-7.195e-02	-8.023e-02
9	7.566e-02	3.990e-02	4.631e-02	6.796e-02	7.575e-02
10	3.907e-02	1.276e-02	2.724e-02	3.342e-02	4.021e-02
11	-2.554e-02	-1.485e-02	-1.889e-02	-2.135e-02	-2.527e-02
12	-7.764e-02	-4.195e-02	-4.876e-02	-6.883e-02	-7.771e-02
13	7.176e-02	3.749e-02	4.350e-02	6.438e-02	7.192e-02
14	1.837e-02	1.183e-02	1.509e-02	1.484e-02	2.029e-02
15	-2.074e-02	-1.395e-02	-1.778e-02	-1.614e-02	-1.951e-02
16	-7.133e-02	-3.956e-02	-4.597e-02	-6.498e-02	-7.151e-02

Table 5.3: Quantity of interest $\mathbf{Q}^{\gamma}(\mathbf{u})$ for a deterministic problem, applying three enhancements

i	$\mathbf{Q}_i^{\gamma}(\mathbf{u})$	$\mathbf{Q}_i^{\gamma}(\mathbf{u}_0)$	$\mathbf{Q}_i^{\gamma}(\mathbf{u}_1)$	$\mathbf{Q}_i^{\gamma}(\mathbf{u}_2)$	$\mathbf{Q}_i^{\gamma}(\mathbf{u}_3)$
1	-4.078e-02	-2.386e-02	-1.385e-02	-3.440e-02	-4.094e-02
2	-2.967e-02	-1.458e-02	-1.974e-02	-1.879e-02	-2.931e-02
3	-3.273e-02	-1.521e-02	-2.072e-02	-2.009e-02	-3.251e-02
4	-4.665e-02	-2.535e-02	-1.523e-02	-3.688e-02	-4.701e-02
5	-1.913e-02	-1.183e-02	-1.709e-02	-8.179e-03	-1.937e-02
6	-5.952e-02	-2.758e-02	-4.596e-02	-4.562e-02	-5.924e-02
7	-5.756e-02	-2.770e-02	-4.622e-02	-4.342e-02	-5.729e-02
8	-2.233e-02	-1.189e-02	-1.711e-02	-1.379e-02	-2.258e-02
9	-2.539e-02	-1.200e-02	-1.976e-02	-2.102e-02	-2.629e-02
10	-7.673e-02	-2.760e-02	-6.274e-02	-6.834e-02	-7.714e-02
11	-5.843e-02	-2.753e-02	-4.651e-02	-5.164e-02	-5.750e-02
12	-2.622e-02	-1.188e-02	-1.955e-02	-1.948e-02	-2.591e-02
13	-2.473e-02	-1.230e-02	-2.062e-02	-2.509e-02	-2.761e-02
14	-5.286e-02	-2.727e-02	-4.608e-02	-5.017e-02	-5.477e-02
15	-5.409e-02	-2.721e-02	-4.599e-02	-4.868e-02	-5.128e-02
16	-2.887e-02	-1.222e-02	-2.049e-02	-2.099e-02	-2.682e-02

Table 5.4: Total and relative errors in quantity of interest $\mathbf{Q}^x(\mathbf{u})$ for homogenized solution

i	$\mathbf{Q}_i^x(\mathbf{u}) - \mathbf{Q}_i^x(\mathbf{u}_0)$	$\frac{\mathbf{Q}_i^x(\mathbf{u}) - \mathbf{Q}_i^x(\mathbf{u}_0)}{\mathbf{Q}_i^x(\mathbf{u})}$ (%)
1	-1.222e-01	42.628
2	-3.158e-02	38.991
3	4.032e-02	41.549
4	1.238e-01	41.819
5	-1.253e-01	44.154
6	-2.954e-02	36.841
7	3.881e-02	39.891
8	1.240e-01	42.751
9	-1.227e-01	45.050
10	-8.124e-02	63.088
11	3.549e-02	39.035
12	1.179e-01	42.823
13	-1.132e-01	44.549
14	-2.450e-02	35.560
15	3.724e-02	41.611
16	1.087e-01	42.242

Table 5.5: Total and relative errors in quantity of interest $\mathbf{Q}^y(\mathbf{u})$ for homogenized solution

i	$\mathbf{Q}_i^y(\mathbf{u}) - \mathbf{Q}_i^y(\mathbf{u}_0)$	$\frac{\mathbf{Q}_i^y(\mathbf{u}) - \mathbf{Q}_i^y(\mathbf{u}_0)}{\mathbf{Q}_i^y(\mathbf{u})}$ (%)
1	2.365e-02	41.722
2	3.328e-03	32.193
3	-4.657e-03	37.393
4	-2.377e-02	40.860
5	3.832e-02	47.725
6	7.901e-03	37.615
7	-7.326e-03	32.950
8	-3.625e-02	45.199
9	3.576e-02	47.268
10	2.631e-02	67.341
11	-1.069e-02	41.861
12	-3.570e-02	45.973
13	3.427e-02	47.763
14	6.536e-03	35.586
15	-6.791e-03	32.748
16	-3.178e-02	44.545

Table 5.6: Total and relative errors in quantity of interest $\mathbf{Q}^{\gamma}(\mathbf{u})$ for homogenized solution

i	$\mathbf{Q}_i^{\gamma}(\mathbf{u}) - \mathbf{Q}_i^{\gamma}(\mathbf{u}_0)$	$\frac{\mathbf{Q}_i^{\gamma}(\mathbf{u}) - \mathbf{Q}_i^{\gamma}(\mathbf{u}_0)}{\mathbf{Q}_i^{\gamma}(\mathbf{u})}$ (%)
1	-1.692e-02	41.484
2	-1.509e-02	50.870
3	-1.752e-02	53.532
4	-2.130e-02	45.659
5	-7.301e-03	38.154
6	-3.194e-02	53.668
7	-2.986e-02	51.880
8	-1.043e-02	46.739
9	-1.339e-02	52.745
10	-4.913e-02	64.031
11	-3.091e-02	52.892
12	-1.434e-02	54.696
13	-1.243e-02	50.261
14	-2.559e-02	48.412
15	-2.688e-02	49.698
16	-1.665e-02	57.669

Table 5.7: Total and relative errors in quantity of interest $\mathbf{Q}^x(\mathbf{u})$ for three enhancements

i	$\mathbf{Q}_i^x(\mathbf{u}) - \mathbf{Q}_i^x(\mathbf{u}_1)$	$\frac{\mathbf{Q}_i^x(\mathbf{u}) - \mathbf{Q}_i^x(\mathbf{u}_1)}{\mathbf{Q}_i^x(\mathbf{u})}$ (%)	$\mathbf{Q}_i^x(\mathbf{u}) - \mathbf{Q}_i^x(\mathbf{u}_2)$	$\frac{\mathbf{Q}_i^x(\mathbf{u}) - \mathbf{Q}_i^x(\mathbf{u}_2)}{\mathbf{Q}_i^x(\mathbf{u})}$ (%)	$\mathbf{Q}_i^x(\mathbf{u}) - \mathbf{Q}_i^x(\mathbf{u}_3)$	$\frac{\mathbf{Q}_i^x(\mathbf{u}) - \mathbf{Q}_i^x(\mathbf{u}_3)}{\mathbf{Q}_i^x(\mathbf{u})}$ (%)
1	-4.137e-02	14.435	-2.945e-02	10.277	-7.955e-05	0.028
2	-1.772e-02	21.884	1.483e-02	-18.309	2.236e-04	-0.276
3	2.443e-02	25.176	-1.079e-02	-11.120	-1.846e-04	-0.190
4	3.929e-02	13.275	2.563e-02	8.659	-1.310e-05	-0.004
5	-3.943e-02	13.900	-2.610e-02	9.202	9.382e-05	-0.033
6	-1.147e-02	14.308	9.090e-03	-11.336	9.465e-05	-0.118
7	1.799e-02	18.491	-1.167e-02	-11.996	-2.263e-04	-0.233
8	3.424e-02	11.803	2.595e-02	8.946	1.115e-04	0.038
9	-4.009e-02	14.714	-2.162e-02	7.935	-2.174e-04	0.080
10	-3.780e-02	29.351	1.016e-02	-7.888	1.015e-03	-0.788
11	1.525e-02	16.779	-1.051e-02	-11.560	1.515e-04	0.167
12	3.120e-02	11.334	2.212e-02	8.036	-1.935e-04	-0.070
13	-3.517e-02	13.841	-2.100e-02	8.262	-1.042e-03	0.410
14	-8.233e-03	11.949	7.020e-03	-10.189	1.841e-03	-2.671
15	1.813e-02	20.254	-6.587e-03	-7.361	9.226e-04	1.031
16	2.661e-02	10.338	1.772e-02	6.884	-9.318e-04	-0.362

Table 5.8: Total and relative errors in quantity of interest $\mathbf{Q}^y(\mathbf{u})$ with three enhancements

i	$\mathbf{Q}_i^y(\mathbf{u}) - \mathbf{Q}_i^y(\mathbf{u}_1)$	$\frac{\mathbf{Q}_i^y(\mathbf{u}) - \mathbf{Q}_i^y(\mathbf{u}_1)}{\mathbf{Q}_i^y(\mathbf{u})}$ (%)	$\mathbf{Q}_i^y(\mathbf{u}) - \mathbf{Q}_i^y(\mathbf{u}_2)$	$\frac{\mathbf{Q}_i^y(\mathbf{u}) - \mathbf{Q}_i^y(\mathbf{u}_2)}{\mathbf{Q}_i^y(\mathbf{u})}$ (%)	$\mathbf{Q}_i^y(\mathbf{u}) - \mathbf{Q}_i^y(\mathbf{u}_3)$	$\frac{\mathbf{Q}_i^y(\mathbf{u}) - \mathbf{Q}_i^y(\mathbf{u}_3)}{\mathbf{Q}_i^y(\mathbf{u})}$ (%)
1	1.783e-02	31.463	6.760e-03	11.928	-2.591e-05	-0.046
2	3.938e-03	38.091	-9.871e-04	-9.549	-5.817e-05	-0.563
3	-5.457e-03	43.819	1.211e-04	-0.972	1.890e-04	-1.518
4	-1.771e-02	30.436	-5.941e-03	10.212	9.049e-05	-0.156
5	3.172e-02	39.501	8.388e-03	10.446	-1.254e-04	-0.156
6	4.600e-03	21.899	1.434e-03	6.825	-2.135e-04	-1.017
7	-3.631e-03	16.330	5.492e-04	-2.470	7.855e-05	-0.353
8	-2.928e-02	36.514	-8.246e-03	10.283	3.763e-05	-0.047
9	2.934e-02	38.784	7.703e-03	10.181	-9.138e-05	-0.121
10	1.183e-02	30.271	5.649e-03	14.459	-1.140e-03	-2.919
11	-6.646e-03	26.022	-4.194e-03	16.422	-2.722e-04	1.066
12	-2.888e-02	37.195	-8.815e-03	11.353	6.743e-05	-0.087
13	2.826e-02	39.382	7.385e-03	10.291	-1.550e-04	-0.216
14	3.279e-03	17.854	3.530e-03	19.218	-1.924e-03	-10.476
15	-2.962e-03	14.285	-4.597e-03	22.168	-1.225e-03	5.909
16	-2.536e-02	35.552	-6.349e-03	8.900	1.771e-04	-0.248

Table 5.9: Total and relative errors in quantity of interest $\mathbf{Q}^\gamma(\mathbf{u})$ with three enhancements

i	$\mathbf{Q}_i^\gamma(\mathbf{u}) - \mathbf{Q}_i^\gamma(\mathbf{u}_1)$	$\frac{\mathbf{Q}_i^\gamma(\mathbf{u}) - \mathbf{Q}_i^\gamma(\mathbf{u}_1)}{\mathbf{Q}_i^\gamma(\mathbf{u})}$ (%)	$\mathbf{Q}_i^\gamma(\mathbf{u}) - \mathbf{Q}_i^\gamma(\mathbf{u}_2)$	$\frac{\mathbf{Q}_i^\gamma(\mathbf{u}) - \mathbf{Q}_i^\gamma(\mathbf{u}_2)}{\mathbf{Q}_i^\gamma(\mathbf{u})}$ (%)	$\mathbf{Q}_i^\gamma(\mathbf{u}) - \mathbf{Q}_i^\gamma(\mathbf{u}_3)$	$\frac{\mathbf{Q}_i^\gamma(\mathbf{u}) - \mathbf{Q}_i^\gamma(\mathbf{u}_3)}{\mathbf{Q}_i^\gamma(\mathbf{u})}$ (%)
1	-2.693e-02	66.042	-6.374e-03	15.631	1.598e-04	-0.392
2	-9.935e-03	33.483	-1.088e-02	36.667	-3.590e-04	1.210
3	-1.202e-02	36.707	-1.265e-02	38.636	-2.204e-04	0.673
4	-3.142e-02	67.348	-9.772e-03	20.948	3.607e-04	-0.773
5	-2.048e-03	10.701	-1.096e-02	57.255	2.352e-04	-1.229
6	-1.356e-02	22.788	-1.390e-02	23.354	-2.794e-04	0.469
7	-1.134e-02	19.701	-1.414e-02	24.568	-2.686e-04	0.467
8	-5.214e-03	23.357	-8.531e-03	38.213	2.574e-04	-1.153
9	-5.632e-03	22.181	-4.370e-03	17.210	9.047e-04	-3.563
10	-1.399e-02	18.230	-8.386e-03	10.930	4.197e-04	-0.547
11	-1.192e-02	20.401	-6.796e-03	11.631	-9.293e-04	1.590
12	-6.665e-03	25.421	-6.743e-03	25.717	-3.072e-04	1.172
13	-4.106e-03	16.608	3.631e-04	-1.469	2.886e-03	-11.671
14	-6.774e-03	12.816	-2.685e-03	5.080	1.907e-03	-3.608
15	-8.104e-03	14.983	-5.408e-03	9.997	-2.811e-03	5.197
16	-8.380e-03	29.023	-7.880e-03	27.291	-2.052e-03	7.107

Table 5.10: Estimates of enhancement errors in quantity of interest $\mathbf{Q}^x(\mathbf{u})$ based on η_0 using three enhancements with effectivity indices

i	η_0^x	$\frac{\eta_0^x}{\mathbf{Q}_i^x(\mathbf{u})-\mathbf{Q}_i^x(\mathbf{u}_0)}$	$\eta_{0,1}^x$	$\frac{\eta_{0,1}^x}{\mathbf{Q}_i^x(\mathbf{u})-\mathbf{Q}_i^x(\mathbf{u}_1)}$	$\eta_{0,2}^x$	$\frac{\eta_{0,2}^x}{\mathbf{Q}_i^x(\mathbf{u})-\mathbf{Q}_i^x(\mathbf{u}_2)}$
1	-1.560e-01	1.277	-7.521e-02	1.818	-6.330e-02	2.149
2	-4.671e-02	1.479	-3.285e-02	1.854	-3.006e-04	-0.020
3	5.358e-02	1.329	3.769e-02	1.543	2.473e-03	-0.229
4	1.634e-01	1.320	7.889e-02	2.008	6.523e-02	2.545
5	-1.530e-01	1.222	-6.723e-02	1.705	-5.390e-02	2.065
6	-4.885e-02	1.654	-3.079e-02	2.683	-1.022e-02	-1.125
7	5.637e-02	1.453	3.555e-02	1.976	5.894e-03	-0.505
8	1.604e-01	1.294	7.065e-02	2.063	6.236e-02	2.403
9	-1.449e-01	1.181	-6.226e-02	1.553	-4.379e-02	2.026
10	-1.048e-01	1.290	-6.137e-02	1.624	-1.341e-02	-1.321
11	5.363e-02	1.511	3.340e-02	2.190	7.637e-03	-0.727
12	1.524e-01	1.292	6.568e-02	2.105	5.660e-02	2.558
13	-1.364e-01	1.205	-5.837e-02	1.659	-4.419e-02	2.105
14	-4.298e-02	1.754	-2.671e-02	3.244	-1.146e-02	-1.632
15	5.058e-02	1.358	3.147e-02	1.736	6.755e-03	-1.026
16	1.439e-01	1.324	6.179e-02	2.322	5.290e-02	2.985

Table 5.11: Estimates of enhancement errors in quantity of interest $\mathbf{Q}^y(\mathbf{u})$ based on η_0 using three enhancements with effectivity indices

i	η_0^y	$\frac{\eta_0^y}{\mathbf{Q}_i^y(\mathbf{u})-\mathbf{Q}_i^y(\mathbf{u}_0)}$	$\eta_{0,1}^y$	$\frac{\eta_{0,1}^y}{\mathbf{Q}_i^y(\mathbf{u})-\mathbf{Q}_i^y(\mathbf{u}_1)}$	$\eta_{0,2}^y$	$\frac{\eta_{0,2}^y}{\mathbf{Q}_i^y(\mathbf{u})-\mathbf{Q}_i^y(\mathbf{u}_2)}$
1	5.597e-02	2.367	5.016e-02	2.813	3.909e-02	5.782
2	1.466e-02	4.404	1.527e-02	3.877	1.034e-02	-10.475
3	-1.660e-02	3.564	-1.740e-02	3.188	-1.182e-02	-97.624
4	-5.846e-02	2.459	-5.240e-02	2.959	-4.063e-02	6.838
5	6.504e-02	1.697	5.844e-02	1.842	3.511e-02	4.185
6	2.048e-02	2.592	1.717e-02	3.734	1.401e-02	9.772
7	-2.344e-02	3.199	-1.974e-02	5.437	-1.556e-02	-28.336
8	-6.812e-02	1.879	-6.116e-02	2.088	-4.012e-02	4.865
9	6.189e-02	1.731	5.548e-02	1.891	3.384e-02	4.393
10	3.333e-02	1.267	1.885e-02	1.594	1.267e-02	2.243
11	-2.296e-02	2.147	-1.891e-02	2.846	-1.646e-02	3.925
12	-6.508e-02	1.823	-5.826e-02	2.017	-3.820e-02	4.333
13	5.821e-02	1.698	5.219e-02	1.847	3.132e-02	4.241
14	1.835e-02	2.808	1.510e-02	4.604	1.535e-02	4.348
15	-2.162e-02	3.184	-1.779e-02	6.006	-1.943e-02	4.226
16	-6.142e-02	1.933	-5.501e-02	2.169	-3.599e-02	5.669

Table 5.12: Estimates of enhancement errors in quantity of interest $\mathbf{Q}^\gamma(\mathbf{u})$ based on η_0 using three enhancements with effectivity indices

i	η_0^γ	$\frac{\eta_0^\gamma}{\mathbf{Q}_i^\gamma(\mathbf{u})-\mathbf{Q}_i^\gamma(\mathbf{u}_0)}$	$\eta_{0,1}^\gamma$	$\frac{\eta_{0,1}^\gamma}{\mathbf{Q}_i^\gamma(\mathbf{u})-\mathbf{Q}_i^\gamma(\mathbf{u}_1)}$	$\eta_{0,2}^\gamma$	$\frac{\eta_{0,2}^\gamma}{\mathbf{Q}_i^\gamma(\mathbf{u})-\mathbf{Q}_i^\gamma(\mathbf{u}_2)}$
1	-2.352e-02	1.391	-3.354e-02	1.245	-1.298e-02	2.037
2	-1.416e-02	0.938	-9.001e-03	0.906	-9.946e-03	0.914
3	-1.482e-02	0.846	-9.310e-03	0.775	-9.941e-03	0.786
4	-2.499e-02	1.173	-3.510e-02	1.117	-1.346e-02	1.377
5	-1.277e-02	1.749	-7.513e-03	3.669	-1.642e-02	1.499
6	-2.895e-02	0.906	-1.057e-02	0.779	-1.090e-02	0.784
7	-2.908e-02	0.974	-1.056e-02	0.931	-1.336e-02	0.945
8	-1.287e-02	1.233	-7.651e-03	1.467	-1.097e-02	1.286
9	-1.255e-02	0.937	-4.786e-03	0.850	-3.524e-03	0.806
10	-6.323e-02	1.287	-2.809e-02	2.008	-2.249e-02	2.682
11	-2.913e-02	0.943	-1.014e-02	0.851	-5.020e-03	0.739
12	-1.244e-02	0.868	-4.766e-03	0.715	-4.844e-03	0.718
13	-1.278e-02	1.028	-4.459e-03	1.086	1.030e-05	0.028
14	-2.888e-02	1.129	-1.006e-02	1.486	-5.976e-03	2.226
15	-2.882e-02	1.072	-1.004e-02	1.239	-7.345e-03	1.358
16	-1.271e-02	0.763	-4.436e-03	0.529	-3.936e-03	0.500

Table 5.13: Average estimates of enhancement errors in quantity of interest $\mathbf{Q}^x(\mathbf{u})$ using three enhancements with effectivity indices

i	η^x_{avg}	$\frac{\eta^x_{avg}}{\mathbf{Q}^x_i(\mathbf{u})-\mathbf{Q}^x_i(\mathbf{u}_0)}$	$\eta^x_{avg,1}$	$\frac{\eta^x_{avg,1}}{\mathbf{Q}^x_i(\mathbf{u})-\mathbf{Q}^x_i(\mathbf{u}_1)}$	$\eta^x_{avg,2}$	$\frac{\eta^x_{avg,2}}{\mathbf{Q}^x_i(\mathbf{u})-\mathbf{Q}^x_i(\mathbf{u}_2)}$
1	-1.184e-01	0.969	-3.761e-02	0.909	-2.569e-02	0.872
2	-3.028e-02	0.959	-1.643e-02	0.927	1.613e-02	1.087
3	3.473e-02	0.862	1.885e-02	0.771	-1.637e-02	1.517
4	1.239e-01	1.001	3.945e-02	1.004	2.578e-02	1.006
5	-1.194e-01	0.954	-3.361e-02	0.852	-2.029e-02	0.777
6	-3.346e-02	1.133	-1.539e-02	1.342	5.171e-03	0.569
7	3.859e-02	0.995	1.778e-02	0.988	-1.188e-02	1.018
8	1.251e-01	1.009	3.532e-02	1.032	2.704e-02	1.042
9	-1.138e-01	0.927	-3.113e-02	0.777	-1.266e-02	0.586
10	-7.413e-02	0.912	-3.068e-02	0.812	1.727e-02	1.700
11	3.693e-02	1.041	1.670e-02	1.095	-9.063e-03	0.862
12	1.195e-01	1.014	3.284e-02	1.052	2.376e-02	1.074
13	-1.072e-01	0.947	-2.918e-02	0.830	-1.501e-02	0.715
14	-2.962e-02	1.209	-1.335e-02	1.622	1.899e-03	0.270
15	3.485e-02	0.936	1.573e-02	0.868	-8.978e-03	1.363
16	1.130e-01	1.039	3.090e-02	1.161	2.201e-02	1.242

5.2 Initial Extention to Stochastic Problems

This section presents the results of a preliminary investigation into the extension of the local error estimate to include stochastic problems. A model problem similar to that used in the deterministic investigation is used here, with all parameters, dimensions, loads, and material properties remaining the same, with the exception of the material properties of the inclusions. The inclusions for this investigation remain linearly elastic and isotropic, but the Young's Modulus and Poisson's Ratio are *random variables*, occupying a truncated Gaussian distribution: the Young's Modulus varies between $E_{inc}^{min} = 130$ GPa and $E_{inc}^{max} = 170$ GPa, with a statistical mean of $E_{inc}^{avg} = 150$ GPa, and a standard deviation of 28 GPa, and the Poisson's Ratio varies between $\nu_{inc}^{min} = 0.17$ and $\nu_{inc}^{max} = 0.22$, with a statistical mean of $\nu_{inc}^{avg} = 0.20$ and a standard deviation of 0.03. These properties apply for every inclusion in the problem, thus creating a stochastic problem in an two-dimensional probability space. Since the probability space is small in this case, reasonable accuracy for the estimates can be obtained by integrating the probability distribution with a five by five point Gaussian Quadrature rule.

For the error estimate in the stochastic case, one knows that the stochastic solution $\mathbf{u}$ satisfies the following stochastic PDE:

$$-\nabla \cdot \mathbf{E}(\mathbf{x}, \boldsymbol{\omega}) \nabla \mathbf{u}(\mathbf{x}, \boldsymbol{\omega}) = \mathbf{f} \quad \text{in } \Omega \times \mathcal{A} \tag{5.1}$$

where $\mathcal{A}$ is the probability space. Following the approach in Section 4.2, the following is also true:

$$-\nabla \cdot \mathbf{E}(\mathbf{x}, \boldsymbol{\omega}) \nabla \mathbf{u}(\mathbf{x}, \boldsymbol{\omega}) = \mathbf{f} \quad \text{in } \omega \times \mathcal{A} \tag{5.2}$$

and the resulting local variational statement is similarly developed:

$$\begin{aligned}\int_{\mathcal{A}}\int_{\omega}\mathbf{E}(\mathbf{x},\boldsymbol{\omega})\nabla\mathbf{u}\cdot\nabla\mathbf{v}\;\mathrm{d}\mathbf{x}\;\mathrm{d}\mathcal{P} \;&=\; \int_{\mathcal{A}}\int_{\omega}\mathbf{f}\cdot\mathbf{v}\;\mathrm{d}\mathbf{x}\;\mathrm{d}\mathcal{P} \\ &\quad+\int_{\mathcal{A}}\int_{\partial\omega}(\mathbf{E}(\mathbf{x},\boldsymbol{\omega})\nabla\mathbf{u}\mathbf{n}_{\omega})\cdot\mathbf{v}\;\mathrm{d}\mathbf{s}\;\mathrm{d}\mathcal{P} \\ &\quad\forall\mathbf{v}\in\mathbf{H}^{1}(\omega)\end{aligned} \tag{5.3}$$

where $\mathcal{A}$ is the (two-dimensional) probability space and $\mathcal{P}$ is the corresponding probability measure defined on $\mathcal{A}$, *i.e.*:

$$\mathrm{d}\mathcal{P} = p(\boldsymbol{\omega})\;\mathrm{d}\boldsymbol{\omega}$$

where $p(\boldsymbol{\omega})$ is the probability density distribution. Recognizing that the problem is linear in the probability space allows the approach in Section 4.2 to be applied, giving an estimate for the statistical average of the modeling error:

$$\eta_0 = \int_{A}\int_{\omega}\big(\mathbf{E}_0-\mathbf{E}(\mathbf{x},\boldsymbol{\omega})\big)\nabla\mathbf{u}_0\cdot\nabla\mathbf{p}\;\mathrm{d}\mathbf{x}\;\mathrm{d}\mathcal{P} \tag{5.4}$$

This procedure is performed using the average elastic strain in the x-direction, ε_{xx} over ω_8 (see Figure 5.2) as the quantity of interest. The probability space was integrated with the five by five Gaussian Quadrature rule. Two enhancements are subsequently performed in an identical manner to the deterministic approach.

The results of this investigation are presented in Tables 5.14, 5.15, 5.16, 5.17, and 5.18.

This preliminary investigation indicates that the stochastic extension of this error estimation has a performance similar to the estimate used for deterministic problems. The effectivity indices for the estimates are close to unity.

Table 5.14: Quantity of interest $\mathbf{Q}^x(\mathbf{u})$ values for deterministic problem with three enhancements

i	$\mathbf{Q}_i^x(\mathbf{u})$	$\mathbf{Q}_i^x(\mathbf{u}_0)$	$\mathbf{Q}_i^x(\mathbf{u}_1)$	$\mathbf{Q}_i^x(\mathbf{u}_2)$
avg	2.902e-01	1.661e-01	2.559e-01	2.642e-01

Table 5.15: Total and relative errors in quantity of interest $\mathbf{Q}^x(\mathbf{u})$ for homogenized solution

i	$\mathbf{Q}_i^x(\mathbf{u}) - \mathbf{Q}_i^x(\mathbf{u}_0)$	$\frac{\mathbf{Q}_i^x(\mathbf{u}) - \mathbf{Q}_i^x(\mathbf{u}_0)}{\mathbf{Q}_i^x(\mathbf{u})}$ (%)
avg	1.241e-01	42.761

Table 5.16: Total and relative errors in quantity of interest $\mathbf{Q}^x(\mathbf{u})$ for two enhancements

i	$\mathbf{Q}_i^x(\mathbf{u}) - \mathbf{Q}_i^x(\mathbf{u}_1)$	$\frac{\mathbf{Q}_i^x(\mathbf{u}) - \mathbf{Q}_i^x(\mathbf{u}_1)}{\mathbf{Q}_i^x(\mathbf{u})}$ (%)	$\mathbf{Q}_i^x(\mathbf{u}) - \mathbf{Q}_i^x(\mathbf{u}_2)$	$\frac{\mathbf{Q}_i^x(\mathbf{u}) - \mathbf{Q}_i^x(\mathbf{u}_2)}{\mathbf{Q}_i^x(\mathbf{u})}$ (%)
avg	3.425e-02	11.804	2.492e-02	8.618

Table 5.17: Estimates of enhancement errors in quantity of interest $\mathbf{Q}^x(\mathbf{u})$ based on η_0 using two enhancements with effectivity indices

i	η_0^x	$\frac{\eta_0^x}{\mathbf{Q}_i^x(\mathbf{u})-\mathbf{Q}_i^x(\mathbf{u}_0)}$	$\eta_{0,1}^x$	$\frac{\eta_{0,1}^x}{\mathbf{Q}_i^x(\mathbf{u})-\mathbf{Q}_i^x(\mathbf{u}_1)}$	$\eta_{0,2}^x$	$\frac{\eta_{0,2}^x}{\mathbf{Q}_i^x(\mathbf{u})-\mathbf{Q}_i^x(\mathbf{u}_2)}$
avg	1.601e-01	1.290	7.026e-02	2.344	6.198e-02	2.484

Table 5.18: Average estimates of enhancement errors in quantity of interest $\mathbf{Q}^x(\mathbf{u})$ using three enhancements with effectivity indices

i	η_{avg}^x	$\frac{\eta_{avg}^x}{\mathbf{Q}_i^x(\mathbf{u})-\mathbf{Q}_i^x(\mathbf{u}_0)}$	$\eta_{avg,1}^x$	$\frac{\eta_{avg,1}^x}{\mathbf{Q}_i^x(\mathbf{u})-\mathbf{Q}_i^x(\mathbf{u}_1)}$	$\eta_{avg,2}^x$	$\frac{\eta_{avg,2}^x}{\mathbf{Q}_i^x(\mathbf{u})-\mathbf{Q}_i^x(\mathbf{u}_2)}$
avg	1.250e-01	1.007	3.513e-02	1.026	2.684e-02	1.076

Chapter 6

Concluding Remarks and Future Work

In this thesis, a new *local* estimator is presented for estimating modeling error in quantities of interest within the GOAM framework. This new estimator greatly reduces computational expense and increases accuracy over previous global methods [12], which themselves required surrogate models to be computed.

The main accomplishments of this thesis are summarized as follows:

6.1 Major Accomplishments

- **A new residual-based error estimator, involving a *local* dual problem has been developed that can be solved exactly without requiring surrogate models.**

  Previously developed error estimates rely on global dual problems that contain the same level of complexity as the exact problem itself, thus requiring the development of surrogate models for the dual problem. This leads to unnecessary complexity and relatively poor reliability of global-dual-based error estimates. Using the local error estimate bypasses this problem completely, as the full heterogeneity of the material in the local subdomain can be used without the computational expense becoming prohibitive. This means that the dual problem can be solved *exactly*,

greatly incresing accuracy, and consequently, only a single computation needs to be done for a given dual problem, further reducing computational expense over previous methods.

- **The local dual problem and error estimator have been implemented as extensions of the FINESSE finite element analysis system.**

  The FINESSE analysis software used by the Computational Mechanics Program of the Department of Mechanical Engineering at the University of Kansas has been extended to allow the computation of the dual problem using the same computational infrastructure as the primal problem. This allows the data from both simulations to be used transparently in error estimation. This, in turn, enables the use of a wide range of experiments.

- **An initial application of the GOAM method has been implemented.**

  To test the effectivity of the error estimator, the adaptive modeling algorithm based on the GOAM method has been implemented in a computational infrastructure. It involves the construction of a homogenized surrogate model using the average of the upper and lower Hashin-Shtrikman bounds, after which a progressively enhanced series of surrogate models is developed according to the GOAM algorithm. These problems use the global enhancement method as described in Section 3.3.2, and a series of three successive enhancements are used for each domain of interest studied.

- **Experimental results indicate good effectivitys.**

  In the error estimation community, effectivity indices of error estimates are considered good in an approximate range between 0.5 and 3. The error estimate developed here yields error estimates with effectivity indices as good as 1.21 for homogenization error and 1.78 for the first enhancement using η_0 and effectivity indices as good as 1.008 for homogenization error and 1.03 for the first enhancement using η_{avg}. It is also worth noting that the experimental problem, though academic in nature, indicates accurate estimates for a relatively large-scale heterogeneity. In most structural engineering applications, *i.e.* multi-phase composites, the scale (ϵ) of the heterogeneity is much smaller. It is anticipated that in those cases, the proposed estimators have even higher accuracy and better effectivity indices.

- **Estimates of modeling error in enhanced solutions have been performed**

  Error estimates of the modeling error in the enhanced solutions of the GOAM methos, using *global* enhancements, have numerically been investigated. Effectivity indices show good to reasonably good accuracy in estimating enhanced errors.

6.2 Limitations and Future Work

The error estimate developed in this thesis is not without some limitations. These, along with important extensions of this method to encompass a wider array of problems will be addressed in future research. Major focuses of

future research include:

- **Extension of this method to include error estimates based on Least Squares formulations**

  The current method, based on Galerkin Method with Weak Form, is only useful for problems for which this formulation is stable–*i.e.* self-adjoint problems, such as linear elastostatics and steady-state reaction-diffusion problems. To be able to use these methods for non-self-adjoint or non-linear problems, such as those involving plasticity, nonlinear quantities of interest, fluid flow, and time-dependent problems, a Least Squares formulation is required. In addition, the exploration of Least Squares formulations is needed due to the unresolved issues in the error estimation process. Firstly, using a local Least Squares integral formulation for the dual problem potentially could enable the estimation of local quantities of interest in terms of displacements, which is currently impossible in the presented estimation framework. Secondly, the estimation of the error in the enhanced solutions remains to be rigorously addressed. Currently, the estimation of the homogenization error (*i.e.*, using η_0 – see (4.25)) is accurate. There is an inaccuracy in η_0 that is caused by the fact that the traction of the homogenized solution $\mathbf{E}_0\nabla\mathbf{u}_0\mathbf{n}_\omega$ on the boundary of the local domain is only equal to the actual fine-scale traction $\mathbf{E}\nabla\mathbf{u}\mathbf{n}_\omega$ in the average sense, *not pointwise* on $\partial\omega$. This inaccuracy causes the effectivity indices of the estimator to deteriorate when estimating the error of the enhanced solutions. In other words, the inaccuracy in η_0 is of the same order as the actual modeling error in those cases.

One can potentially resolve/estimate the difference between $\mathbf{E}\nabla\mathbf{u}\mathbf{n}_\omega$ and $\mathbf{E}_0\nabla\mathbf{u}_0\mathbf{n}_\omega$. However, in the worst case, these entities belong to $\mathbf{H}^{-\frac{1}{2}}(\partial\omega)$. To achieve bounds or estimates of such terms, one needs H-LaPlacian terms (*i.e.* second-order derivatives) to be included in the local integral formulations. Currently the only way to do this is by using a Least Squares approach.

- **Investigation into local methods of enhancement**

  Sections 3.3.1 and 3.3.2 describe current methods of enhancing the surrogate model used in this framework, but as described previously, only the global enhancement method currently provides an accurate simulation, due to the decoupling inherent in the local enhancement method. Thus, only global enhancements were used in the scope of this thesis, but a further investigation into improvements in the local enhancement method, specifically the exploration of strain compatibility equations, is warranted.

- **Extension of this method to stochastic problems**

  This thesis assumes that the material properties of the constituents of the composite are deterministic. However, in nearly all practical applications of composite materials, the constituent material properties vary widely and are generally known only in a statistical sense. Additionally, it is generally impossible to know the exact global composite geometry of real-world structures. To improve the simulation of real composite structures, it is necessary to expand this method to include multiple dimensions of stochastic behavior, using either Gaussian Quadrature

integration of the probability space for relatively simple problems, or Monte-Carlo simulations for more complex problems. An initial investigation into this area is presented in Section 5.2, but further research and developments are needed.

Appendix

Appendix 1

Development of Homogenized Material Properties

This appendix presents the method used to determine homogenized surrogate material properties for use in Step 2 of the GOAM framework as used in Chapter 5. The surrogate properties presented here represent the average of the upper and lower Hashin-Shtrikman bounds [8].

To determine the homogenized properties, the material properties and respective volume fractions (V) of the inclusions and matrix must be known. Any complete material description will suffice–this presentation uses Young's Modulus (E) and Poisson Ratio (ν) as well as Bulk Modulus (k) and Shear Modulus (μ).

To begin, it is assumed that the constituent material properties are given in terms of Young's Modulus and Poisson Ratio. The first step is to convert these properties into Bulk Modulus and Shear Modulus. These relations are given by:

$$\mu_{inc} = \frac{E_{inc}}{2(1+\nu_{inc})} \qquad \mu_{mat} = \frac{E_{mat}}{2(1+\nu_{mat})}$$
$$k_{inc} = \frac{E_{inc}}{3(1-2\nu_{inc})} \qquad k_{mat} = \frac{E_{mat}}{3(1-2\nu_{mat})}$$

For efficiency of notation, the following terms are used:

$$K_{inc} = k_{inc} + \frac{\mu_{inc}}{3} \qquad K_{mat} = k_{mat} + \frac{\mu_{mat}}{3}$$

Then the following upper and lower bounds on K_0 and μ_0 are given:

$$K_0^- = K_{mat} + \frac{V_{inc}}{\frac{1}{K_{inc}-K_{mat}} + \frac{V_{mat}}{K_{mat}+\mu_{mat}}}$$

$$K_0^+ = K_{inc} + \frac{V_{mat}}{\frac{1}{K_{mat}-K_{inc}} + \frac{V_{inc}}{K_{inc}+\mu_{inc}}}$$

$$\mu_0^- = \mu_{mat} + \frac{V_{inc}}{\frac{1}{\mu_{inc}-\mu_{mat}} + \frac{V_{mat}(K_{mat}+2\mu_{mat})}{2\mu_{mat}(K_{mat}+\mu_{mat})}}$$

$$\mu_0^+ = \mu_{inc} + \frac{V_{mat}}{\frac{1}{\mu_{mat}-\mu_{inc}} + \frac{V_{inc}(K_{inc}+2\mu_{inc})}{2\mu_{inc}(K_{inc}+\mu_{inc})}}$$

In this work, the average of these upper and lower bounds is selected:

$$K_0 = \frac{1}{2}(K_0^- + K_0^+)$$

$$\mu_0 = \frac{1}{2}(\mu_0^- + \mu_0^+)$$

This then gives a homogenized bulk modulus:

$$k_0 = K_0 - \frac{\mu_0}{3}$$

and in turn, the homogenized Young's Modulus is given by:

$$E_0 = \frac{9k_0\mu_0}{3k_0 + \mu_0}$$

and the Poisson Ratio is given by:

$$\nu_0 = \frac{3k_0 - 2\mu_0}{2(3k_0 + \mu_0)}$$

Bibliography

[1] Balendran, B., and Nemat-Nasser, S. Bounds on elastic moduli of composites. *Journal of Mechanics, Physics and Solids 43* (1995), 1825–1853.

[2] Bensoussan, A., Lions, J. L., and Papanicolaou, G. Asymptotic analysis for periodic structures. In *Studies in Mathematics and its Applications*, vol. 5. 1978.

[3] Fu, Y., Klimkowski, K. J., Rodin, G. J., Berger, E., Browne, J. C., Singer, J. K., van de Gein, R. A., and Vemaganti, K. A fast solution method for three-dimensional many particle problems of linear elasticity. *International Journal for Numerical Methods in Engineering 42* (1998), 1215–1229.

[4] Ghosh, S., Lee, K., and Moorthy, S. Two scale analysis of heterogeneous elastic-plastic materials with asymptotic homogenization and voronoi cell finite element method. *Computer Methods in Applied Mechanics and Engineering 132* (1996), 63–116.

[5] Ghosh, S., and Liu, Y. Voronoi cell finite element model based on micropolar theory of thermoelasticity for heterogeneous materials. *International Journal for Numerical Methods in Engineering 38* (1995), 1361–1398.

[6] Ghosh, S., and Moorthy, S. Elastic-plastic analysis of arbitrary heterogeneous materials with the voronoi cell finitte element method. *Computer Methods in Applied Mechanics and Engineering 121* (1995), 373–409.

[7] Guedes, J. M., and Kikuchi, N. Preprocessing and postprocessing for materials based on the homogenization method with adaptive finite element methods. *Computer Methods in Applied Mechanics and Engineering 83* (1990).

[8] Hashin, Z. Analysis of composite materials, a survey. *Journal of Applied Mechanics 50* (1983), 481–505.

[9] Herakovich, C. T. *Mechanics of Fibrous Composites.* John Wiley and Sons, New York, 1998.

[10] Hill, R. The elastic behavior of crystalline aggregate. In *Proc. Phys. Soc. London* (1952), vol. 65, pp. 349–354.

[11] Nemat-Nasser, S., and Hori, M. Universal bounds for overall properties of linear and nonlinear heterogeneous solids. *J. Engng. Mat. Tech 117* (1995), 412–432.

[12] Oden, J. T., and Prudhomme, S. Estimation of modeling error in computational mechanics. *Journal of Computational Physics 146* (2002), 491–519.

[13] Oden, J. T., and Prudhomme, S. Computable error estimators and adaptive techniques for fluid flow problems. In *Lecture Notes in Com-*

putational Science and Engineering, T. J. Barth and H. Deconinck, Eds., vol. 25. Springer Verlag, 2003, pp. 207–268.

[14] Oden, J. T., Prudhomme, S., Romkes, A., and Bauman, P. T. Multiscale modeling of physical phenomena: Adaptive control of models. *SIAM Journal on Scientific Computing 28*, 6 (2006), 2359–2389.

[15] Oden, J. T., and Vemaganti, K. Adaptive modeling of composite structures : Modeling error estimation. *Int. J. Comp. Civil Str. Engrg.* (2000), 1–16.

[16] Oden, J. T., and Vemaganti, K. Estimation of local modeling error and goal-oriented modeling of heterogeneous materials; part i. error estimates and adaptive algorithms. *Journal of Computational Physics 164* (2000), 22–47.

[17] Oden, J. T., and Zohdi, T. I. Analysis and adaptive modeling of highly heterogeneous elastic structures. *Computer Methods in Applied Mechanics and Engineering 148* (1997), 367–391.

[18] Sanchez-Palencia, E. Nonhomogeneous media and vibration theory. vol. 127. Springer Verlag, 1980.

[19] Terada, K., and Kikuchi, N. Nonlinear homogenization method for practical applications. In *Computational Methods in Micromechanics*, S. Ghosh and M. Ostoja-Starzewski, Eds., vol. 212. ASMD AMD, 1995, pp. 1–16.

[20] Terada, K., Miura, T., and Kikuchi, N. Digital image based modeling applied to the homogenization analysis of composite materials. *Computational Mechanics 20* (1997), 331–346.

[21] Vemaganti, K. *Goal-Oriented Adaptive Modeling of Heterogeneous Elastic Solids*. PhD thesis, The University of Texas at Austin, 2000.

[22] Vemaganti, K., and Oden, J. T. Estimation of local modeling error and goal-oriented modeling of heterogeneous materials; part ii. a computational environment for adaptive modeling of heterogeneous elastic solids. *Computer Methods in Applied Mechanics and Engineering 190* (2001), 6089–6124.

[23] Zohdi, T. I. *Voronoi Cell Finite Element model based on micropolar theory of thermoelasticity for heterogeneous materials*. PhD thesis, The University of Texas at Austin, 1995.

[24] Zohdi, T. I., Oden, J. T., and Rodin, G. J. Hierarchical modeling of heterogeneous bodies. *Computer Methods in Applied Mechanics and Engineering 138* (1996), 273–298.

Vita

Tristan Moody was born in Lawrence, Kansas, on September 18, 1983, the son of Bob and Patsy Moody. Graduating from Lawrence Free State High School in 2001, he began undergraduate study in Mechanical Engineering at The University of Kansas. During this time he worked as an intern for the Cessna Aircraft Company in Wichita, Kansas, and worked on manufacturing process improvements for the Frito-Lay Company plant in Topeka, Kansas. After graduating with a Bachelor of Science degree in December 2005, he entered the graduate program in Mechanical Engineering at the Univerity of Kansas and continued work toward a Master of Science.

This thesis was typeset with LaTeX[†] by the author.

[†]LaTeX is a document preparation system developed by Leslie Lamport as a special version of Donald Knuth's TeX Program.